European Journal of Pharmacology 959 (2023) 176079

Contents lists available at ScienceDirect

European Journal of Pharmacology

journal homepage: www.elsevier.com/locate/ejphar

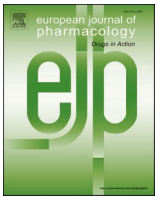

Unravelling a novel role for cannabidivarin in the modulation of subventricular zone postnatal neurogenesis

Diogo M. Lourenço [a,b], Rita Soares [a,b,c], Sónia Sá-Santos [d], Joana M. Mateus [a,b], Rui S. Rodrigues [a,b], João B. Moreira [a,b], Sandra H. Vaz [a,b], Ana M. Sebastião [a,b], Susana Solá [d], Sara Xapelli [a,b,*]

[a] Instituto de Farmacologia e Neurociências, Faculdade de Medicina, Universidade de Lisboa, 1649-028 Lisboa, Portugal
[b] Instituto de Medicina Molecular João Lobo Antunes, Faculdade de Medicina, Universidade de Lisboa, 1649-028 Lisboa, Portugal
[c] Instituto de Biologia Molecular, Faculdade de Medicina, Universidade de Lisboa, 1649-028 Lisboa, Portugal
[d] Research Institute for Medicines (iMed.ULisboa), Faculdade de Farmácia, Universidade de Lisboa, 1649-003 Lisboa, Portugal

ARTICLE INFO

Keywords:
Adult neurogenesis
Cannabidivarin
TRPV1
Neural stem cells
Oligodendrogenesis
Subventricular zone

ABSTRACT

Postnatal neurogenesis has been shown to rely on the endocannabinoid system. Here we aimed at unravelling the role of Cannabidivarin (CBDV), a non-psychoactive cannabinoid, with high affinity for the non-classical cannabinoid receptor TRPV1, on subventricular zone (SVZ) postnatal neurogenesis. Using the neurosphere assay, SVZ-derived neural stem/progenitor cells (NSPCs) were incubated with CBDV and/or 5′-Iodoresinferotoxin (TRPV1 antagonist), and their role on cell viability, proliferation, and differentiation were dissected. CBDV was able to promote, through a TRPV1-dependent mechanism, cell survival, cell proliferation and neuronal differentiation. Furthermore, pulse-chase experiments revealed that CBDV-induced neuronal differentiation was a result of cell cycle exit of NSPCs. Regarding oligodendrocyte differentiation, CBDV inhibited oligodendrocyte differentiation and maturation. Since our data suggested that the CBDV-induced modulation of NSPCs acted via TRPV1, a sodium-calcium channel, and that intracellular calcium levels are known regulators of NSPCs fate and neuronal maturation, single cell calcium imaging was performed to evaluate the functional response of SVZ-derived cells. We observed that CBDV-responsive cells displayed a two-phase calcium influx profile, being the initial phase dependent on TRPV1 activation. Taken together, this work unveiled a novel and untapped neurogenic potential of CBDV via TRPV1 modulation. These findings pave the way to future neural stem cell biological studies and repair strategies by repurposing this non-psychoactive cannabinoid as a valuable therapeutic target.

1. Introduction

Adult neural stem/progenitor cells (NSPCs) can be found in the subventricular zone, (SVZ) lining the lateral walls of the lateral ventricles (Bond et al., 2015). Importantly, adult NSPCs have self-renewing properties and are tri-potent, having the capacity to generate neurons, astrocytes and oligodendrocytes (Soares et al., 2020). In the SVZ, besides originating neuroblasts (Luskin and Boone, 1994), a minority of NSPCs enter the oligodendroglial lineage (Menn et al., 2006; Suzuki and Goldman, 2003) by originating oligodendrocyte progenitor cells (OPCs) that migrate into the surrounding cortex and white matter, differentiating into myelinating oligodendrocytes (Aguirre and Gallo, 2004; Butti et al., 2019).

Adult NSPCs are mostly quiescent *in vivo* (Cavallucci et al., 2016). The balance between quiescence and activity regulates, not only the rate of cytogenesis, but also the long-term maintenance of the NSPC pool (Cheung and Rando, 2013; Urbán et al., 2019). Therefore, finding and exploiting modulators of NSPCs that can boost postnatal neurogenesis and oligodendrogenesis is imperative.

The intricate interplay between the endocannabinoid system and neurogenesis has garnered significant attention in the last decade (Bravo-Ferrer et al., 2017; Ferreira et al., 2018; Galve-Roperh et al., 2013; Molina-Holgado et al., 2007; Rodrigues et al., 2017; Xapelli et al., 2013; Zimmermann et al., 2018). In this work, rather than positioning

* Corresponding author. Instituto de Farmacologia e Neurociências, Faculdade de Medicina, Universidade de Lisboa and Instituto de Medicina Molecular João Lobo Antunes, Faculdade de Medicina, Universidade de Lisboa, 1649Lisboa, Portugal.
E-mail address: sxapelli@medicina.ulisboa.pt (S. Xapelli).

https://doi.org/10.1016/j.ejphar.2023.176079
Received 6 July 2023; Received in revised form 21 September 2023; Accepted 25 September 2023
Available online 5 October 2023

our study to research on classical cannabinoid receptors, we focused on exploring the potential of non-classical cannabinoid receptors, specifically the transient receptor potential cation channel subfamily V member 1 (TRPV1). This sodium-calcium ion channel receptor is integral to processes like thermoregulation and nociception (Caterina et al., 1997; Tominaga and Tominaga, 2005). Importantly, several studies demonstrated that TRPV1 is a potential target for the regulation of cell proliferation and apoptosis (Czaja et al., 2008; Kong et al., 2010; Stock et al., 2014). Previous works have highlighted that, in both mouse and rat models, TRPV1-activation was shown to promote cell death, inhibited of cell proliferation and impaired neuronal maturation (Czaja et al., 2008; Kong et al., 2010). Accordingly, TRPV1 knockout (KO) mice present higher levels of NSPC proliferation when compared to wild type (Stock et al., 2014). In contrast, other works reported a TRPV1-dependent increase of neuronal differentiation and promotion of axonal and neurite growth in dorsal root ganglia cultures (Frey et al., 2018; Goswami et al., 2007). Interestingly, cannabidivarin (CBDV), a non-psychoactive cannabinoid with negligible affinity for cannabinoid type 1 and 2 receptors (CB1R and CB2R) has been described as a TRPV1 agonist (Hill et al., 2013; Rosenthaler et al., 2014). However, CBDV displays versatility by encompassing interactions with several other receptors. In fact, CBDV has been described as an agonist of TRPV2 and TRPA1 (De Petrocellis et al., 2011), as an inverse agonist of GPR6 (Laun et al., 2019) as well as an allosteric antagonist of GPR55 (Anavi-Goffer et al., 2012). However, mounting evidence suggests that CBDV's biological activity primarily operates through a TRPV1-dependent mechanism (Huizenga et al., 2019; Iannotti et al., 2014; Muller et al., 2019; Straiker et al., 2021; Thornton et al., 2020).

Given the role of TRPV1 in regulating cell death, cell proliferation and neuronal differentiation and, that CBDV is a non-psychoactive cannabinoid, it is relevant to thoroughly understand how this emerging cannabinoid can modulate neurogenesis and how it could be used as a viable drug for brain repair strategies. Therefore, with this work we aimed at unravelling how CBDV modulate NSPCs fate and whether those effects are mediated by TRPV1.

2. Material and methods

2.1. Animals

C57BL/6J females were kept in standard housing, grouped in pairs, while males were single housed. All animals were kept on a 12h light/dark cycle, with food and water provided *ad libitum*. No breeding attempts were made before sexual maturity was reached, at 8 weeks of age. Breeding trios were used until one-year old of age or 10 successful mating sessions, in order to maximise breeding success.

All efforts were made to minimize animal suffering and stress, and to use the minimum number of animals, according to standard and ethical procedures. All animals were given access to hiding places, in the form of disposable igloos or cardboard tubes, as well as proper nesting material and wooden pellets for chewing.

Experiments were performed *ex-vivo* with biological material obtained from postnatal day 1–3 (P1-3) C57BL/6J mice and subsequently maintained in *vitro* conditions. A minimum of 3 pups was required to perform one SVZ cell culture and a minimum of 3 independent cultures was required to perform statistical analysis. All pups per litter were used per SVZ cell culture.

2.2. SVZ cell cultures

SVZ Neurospheres (3D clusters of clones of NSPCs) were prepared from early postnatal (P1-3) C57BL/6J mice as previously described (Soares et al., 2020). In brief, P1-3 C57BL/6J mice were decapitated with a single incision with sharp scissors at the base of the brainstem. SVZ fragments were dissected out from 450 μm-thick coronal brain slices. All collected tissue was pooled and digested with 0.05% Trypsin-EDTA (#25300054, Thermo Fisher Scientific) in Hanks' Balanced Salt Solution (HBSS, #14175095, Thermo Fisher Scientific) and mechanically dissociated with a P1000 pipette. Single-cell suspension was resuspended in serum-free medium (SFM), composed of Dulbecco's Modified Eagle Medium/Nutrient Mixture F-12 + GlutaMAX™ supplement (DMEM + GlutaMAX™, #31331028, Thermo Fisher Scientific) supplemented with 100U/mL penicillin and 100 μg/mL streptomycin (#15070063, Thermo Fisher Scientific), 1% B-27™ (#17504044, Thermo Fisher Scientific) and growth factors (10 ng/mL mouse epidermal growth factor (EGF, #53003-018, Thermo Fisher Scientific) and 5 ng/mL human fibroblast growth factor-2 (bFGF-2, #13256-029, Thermo Fisher Scientific)) (proliferative conditions). SVZ cells were seeded in 60 mm diameter Petri dishes (#430166, Corning) and maintained for six days in a 95% air/5% CO_2 humified atmosphere at 37 °C. Resulting neurospheres were seeded for 24h onto 12 mm ⌀ glass coverslips (#631-1577P, VWR) coated with 100 μg/mL poly-D-lysine (PDL, #P7886, Sigma-Aldrich) in SFM devoid of growth factors (differentiative conditions). After 24h (day 0), the medium was renewed with or without (control) a range of pharmacological treatments for 48h or 7 days.

2.3. Pharmacological treatments and experimental setting

Since CBDV has very weak affinity for both CB1R and CB2R (Rosenthaler et al., 2014) and it has been proposed to activate TRPV1 (Iannotti et al., 2014), we evaluated its effects on SVZ-derived NSPC survival, proliferation and differentiation and studied TRPV1-dependency using a selective TRPV1 antagonist (5′-Iodoresiniferatoxin, 5′-IRTX).

Plated neurospheres were exposed to three increasing concentrations of CBDV (drug concentration-response studies) (Table 1). These were established based on previous studies with cannabinoids (Compagnucci et al., 2013; Rodrigues et al., 2017; Stanslowsky et al., 2017; Xapelli et al., 2013) since the Ki for CBDV for TRPV1 is not known. Additionally, to study if the effect seen by CBDV was TRPV1-dependent, the TRPV1 antagonist 5′-IRTX was used. This drug is a potent vanilloid receptor antagonist, 40-fold more potent than the prototypical TRPV1 antagonist capsazepine (Wahl et al., 2001). Whenever cells needed to be co-treated with the antagonist (at 300 nM), they were incubated 30 min prior to the treatment with CBDV. All drugs were dissolved in Dimethyl sulfoxide (DMSO, #D2650, Merck Life Sciences) at a stock solution of 50 mM CBDV and 10 mM 5′-IRTX. Fresh dilutions were prepared on the day of the pharmacological tests with SFM-DMEM + GlutaMAX™ devoid of growth factors.

2.4. Total RNA isolation and quantitative real-time reverse transcription polymerase chain reaction (qRT-PCR)

Total RNA was isolated from DIV7 SVZ-derived cells, subjected to the pharmacological treatments mentioned above, using TRIzol™ Reagent (#15596026, Invitrogen™) (Vilain et al., 2012). Cells were scraped into a tube containing 1 mL TRIzol™ and manually dissociated with a P1000 pipette After mixing with 200 μL of chloroform, and vortexing for 15 s, a centrifugation at 12,000×*g* for 10 min at 4 °C was performed to collect the aqueous phase, to which equal volume of isopropyl alcohol was added. After a centrifugation at 17,500×*g*, for 10 min at 4 °C, RNA pellet was washed in sequential cycles of decreasing volumes of 75% ethanol (400μL–100μL). RNA pellet was air dried, for 15 min at room temperature (RT) and resuspended in 10 μL of nuclease-free water followed by an incubation for 10 min at 55 °C. RNA purity and concentration were obtained using Nanodrop 2000 Spectrophotometer (NanoDrop Technologies LLC). DNA contaminations were eliminated with DNase I recombinant (#04716728001; Roche Applied Science) following the manufacturer's instructions. All samples were stored at −80 °C until use.

cDNA was prepared from 1000 ng total RNA using NZY Reverse Transcriptase (#MB12402; NZYTech) according to manufacturer's

Table 1
Pharmacological treatments.

Drug	Purity	Biological Activity	Concentration used	Ki for CB1R/ CB2R	Ki for TRPV1	Company	#	References
Cannabidivarin 2-((1S,6S)-3-methyl-6-(prop-1-en-2-yl) cyclohex-2-enyl)-5-propylbenzene-1,3-diol	≥98%	TRPV1 agonist and GPR55 antagonist	100 nM 300 nM 1 μM	CB1R: 14711 nM CB2R: 574.2 nM	Not Known	THC Pharm GmbH The Health Concept	–	(Anavi-Goffer et al., 2012; Iannotti et al., 2014; Rosenthaler et al., 2014)
5′-Iodoresiniferatoxin 6,7-Deepoxy-6,7-didehydro-5-deoxy-21-dephenyl-21-(phenylmethyl)-daphnetoxin,20-(4-hydroxy-5-iodo-3-methoxybenzene acetate)	>99%	TRPV1 antagonist	300 nM	Not applicable	5.8 nM	Alomone Labs	I-800	Wahl et al. (2001)

Table 2
Primers.

Gene		Sequence (5′ to 3′)
Trpv1	FW	ACT CTT ACC ACA CAG CAG CC
	RV	GCC CAA TTT GCA ACC AGC TA
Mki67	FW	CCT TTG CTG TCC CCG AAG A
	RV	GGC TTC TCA TCT GTT GCT TCC T
Tubb3	FW	GTG AAG TCA GCA TGA GGG AGA T
	RV	AGG TTC CAA GTC CAC CAG AAT
Gapdh	FW	CCC CTT CAT TGA CCT CAA CTA C
	RV	CCT CAC CCC ATT TGA TGT TAG T

instructions. Real-time RT-PCR was performed using a SensiFastTM SYBR® Hi-ROX kit (#BIO-92020; Bioline USA Inc.) in an Applied Biosystems QuantStudio 7 Flex Real-Time PCR system (Thermo Fisher Scientific Inc.). Primer sequences are listed in Table 2. Relative gene expression was calculated based on the standard curve and normalized to the level of hypoxanthine glyceraldehyde 3-phosphate dehydrogenase (GAPDH) housekeeping gene and expressed as fold change from controls. Primers were designed using the Reference Genome GRCm39 (Ensembl Assembly Genome C57BL_6NJ_v1; Accession: GCA_001632555.1) taken from the Ensembl Release 100 (April 2020).

2.5. Evaluation of cell viability, cell proliferation and cell differentiation under differentiative conditions and immunocytochemistry (ICC) assays

2.5.1. Cell viability

To investigate the effect of the different pharmacological treatments on cell viability, SVZ cells were exposed, at DIV2, to 3 μg/mL of propidium iodide (PI, #P4170, Sigma-Aldrich) for 30min before fixation. PI is a fluorescent intercalating agent that binds to DNA in cells that have a compromised cell membrane, thus is useful to differentiate healthy cells from necrotic or late apoptotic cells (Lecoeur, 2002). Cells were processed for ICC, as mentioned in 2.5.5.

2.5.2. Cell proliferation

Cell proliferation was assessed at DIV2 by co-incubating cells with 10 μM of 5-bromo-2′-deoxyuridine (BrdU) (#B5002, Sigma-Aldrich) in the last 4h of the pharmacological treatments. BrdU is a synthetic thymidine analogue able to substitute thymidine in the DNA double chain during the S Phase of the cell cycle (Kee et al., 2002). Cells were prepared for ICC, as mentioned in 2.5.5. BrdU was unmasked by permeabilizing cells in PBS with 1% Triton™ X-100 at RT for 30min. DNA was denatured in 1M HCl for 20min at 37 °C. See antibodies on Table 3.

2.5.3. Cell differentiation

To assess cell differentiation, cells were fixed at two different timepoints, DIV2 and DIV7, and handled for ICC, as mentioned in 2.5.5. Neuronal and oligodendroglial lineages were evaluated using the respective antibodies on Table 3.

2.5.4. Pulse-chase experiments

SVZ-derived cells were given a BrdU pulse for the first 24h of drug treatments followed by a chase of 6 days (without BrdU) in the absence (control) or presence of our pharmacological treatments. 7-Day treated SVZ-derived cells, were fixed and prepared for ICC according to the protocol described in 2.5.5. For antibodies see Table 3.

2.5.5. ICC assay

Cells were fixed in 4% PFA for 30 min and washed with PBS at RT. An

Table 3
Primary and Secondary antibodies.

Primary antibodies				
Antigen	Host	Dilution	Company	#
BrdU	Mouse	1:500	Dako	M0744
NeuN	Rabbit	1:500	Cell Signalling Technology	12943
NeuN	Mouse	1:500	Merck Milipore	MAB377
NG2	Rabbit	1:500	Merck Milipore	B5320
MBP	Rabbit	1:500	Cell Signalling Technology	78896S
Secondary antibodies				
Antigen	**Host**	**Dilution**	**Company**	**#**
Alexa Fluor® 488 anti-rabbit	Donkey	1:500	Life Technologies	A21206
Alexa Fluor® 488 anti-mouse	Donkey	1:500	Life Technologies	A21202
Alexa Fluor® 568 anti-mouse	Donkey	1:500	Life Technologies	A10037
Alexa Fluor® 568 anti-rabbit	Donkey	1:500	Life Technologies	A10042

incubation with PBS with 0.5% Triton X-100 (#X100, Sigma-Aldrich) and 3% bovine serum albumin (BSA, #MB04602, NZYTech) for 1.5h was performed to block nonspecific binding sites, followed by an overnight incubation with the primary antibodies (Table 3). The next day, after several washes with PBS, the corresponding secondary antibodies (Table 3) were incubated for 1h at RT, followed by nuclei counterstaining with Hoechst 33342 (12 μg/mL in PBS, #H1399, Invitrogen™) and mounting in Mowiol fluorescent medium (#324590, Sigma-Aldrich).

2.6. Evaluation of cell proliferation under proliferative conditions

SVZ neurospheres were prepared according to the protocol mentioned in 2.2 by growing SVZ cells in proliferative conditions (SFM supplemented with EGF and bFGF-2) in the presence or absence (control condition) of CBDV (1 μM). SVZ-derived cells were allowed to form neurospheres and the analysis of proliferation occurred after 5 days in culture. Neurosphere size (diameter, D_N, and area, A_N) was used as an indirect indicator of cell proliferation (Mori et al., 2006).

2.7. Microscopy

Immunofluorescence images were captured using an AxioCamMR3 monochrome digital camera (Carl Zeiss Inc.) mounted on a Zeiss Axiovert 200M inverted widefield fluorescence microscope (Carl Zeiss Inc.), with a 40*x* EC Plan-NeoFluar (NA 0.75) objective. Images were obtained using the software AxioVision 4 (Carl Zeiss Inc.), stored and analysed in an uncompressed 8-bit Tiff (.tiff) format. One pixel corresponds to 0.25 μm and the captured image size was 1388 × 1040 pixels.

Phase contrast images of neurospheres were captured using an AxioCam 208c colour digital camera (Carl Zeiss Inc.) mounted on a Zeiss Primovert inverted widefield microscope (Carl Zeiss Inc.), with a 4x Plan Achromat (NA 0.1) Ph0 objective. Images were obtained using the software Zen 3.2 (Blue edition) (Carl Zeiss Inc.), stored and analysed in an uncompressed Carl Zeiss Image (.czi) format. One pixel corresponds to 0.925 μm and the captured image size was 3840 × 2160 pixels.

2.8. Calcium imaging

SVZ-derived cells were cultured as mentioned in 2.2 and cells were seeded in μ-ibidi 8 well plates (#80826, ibidi). The Ca^{2+} imaging assay was performed in SVZ cells 7 days after seeding using a Zeiss Axiovert 135 TV inverted microscope with epifluorescent optics and equipped with a high-speed multiple excitation fluorimetric system (Lambda DG4, with a 175W Xenon arc lamp), according to Marques et al. (2019) and Rodrigues et al. (2017).

Data was recorded by a cooled CCD camera (Photometrics CoolSNAP). Before measurements, cell medium was replaced by warm standard buffer containing 119 mM NaCl, 2 mM Ca^{2+}, 2 mM $MgCl_2$, 5 mM KCl, 25 mM HEPES, pH 7.4 (adjusted with NaOH). Cells were loaded with the Ca^{2+} sensitive dye Fura-2 AM (5 μM, #47989, Life Technologies) for 45min before performing the intracellular calcium measurements. After 45min, Fura-2 AM was removed and replace by warm standard buffer (as described above) and experiments were performed at room temperature.

In order to evaluate the calcium response to the drugs, at 100s, an incubation with 1 μM CBDV was performed for 700s. If the treatments required co-incubation with the antagonist 5′-IRTX, after the incubation with Fura-2 AM and 30min before performing the intracellular calcium measurements, cells were incubated with the antagonist at 300 nM. At 800s, 2 μM Ionomycin was added to record maximum response of cells (data not shown), as a positive control for cell response. Recordings ended after 900s.

Responses were recorded by a ratiometric method, in which image pairs were obtained every 5s by exciting the preparations at 340 and 380 nm. Fura-2 AM has an absorbance at 340 nm if bound to calcium, and at 380 nm if not, while the emission wavelength is maintained at 510 nm. The magnitude of the changes in the emission fluorescence of Fura-2 AM were taken as a measure of the changes in intracellular calcium concentration, as response to the drug stimulation.

2.9. Statistical analysis

Every independent experiment (*n*) corresponds to one independent SVZ neurosphere culture from one litter of C57BL/6J mice at P1-3. A minimum of 3 independent cultures was required to perform statistical analysis. Statistical analyses were performed using GraphPad Prism version 9.0.0 for Windows (GraphPad Software, Inc.), unless stated otherwise. Significance is reported as: ns: $p > 0.05$; *$p < 0.05$; **$p < 0.01$; ***$p < 0.001$; ****$p < 0.0001$ when compared with control. § For comparisons of the co-incubation of drugs against the respective drug.

2.9.1. For qRT-PCR experiments

SVZ-derived cells were grown in triplicates and each independent culture is considered n = 1. Values were normalized to the control expression of GAPDH expression for each experiment. Data presented as Mean ± standard error of the mean (SEM) and the control was set to 1. Statistical significance was obtained using a Two-tailed Unpaired *t*-test.

2.9.2. For the studies of cell viability, cell proliferation, neuronal/oligodendroglial differentiation, and pulse-chase experiments

All experiment measurements were performed at the border of SVZ neurospheres, where migrating cells form a pseudo-monolayer (Soares et al., 2020). Each condition was measured in three different coverslips. Percentages of immunoreactive cells were calculated from cell counts of five independent microscopic fields in each triplicated coverslip (representing n = 1) with a 40x objective (≈100–200 cells per field). All experiments were analysed in a blind fashion and the obtained data was normalized to each corresponding control. Normalisation of data was obtained by transformation using the Y=Y × K function in GraphPad Prism, with K = control group mean/100. Each individual experiment (*n*) was normalized to the respective control for that experiment. Normal distribution of data was tested using the Shapiro-Wilk normality test, for small sized samples ($n < 50$) (Mishra et al., 2019). Data is presented as Mean ± SEM from the indicated number of independent cultures. For drug concentration-response curve experiments, statistical significance was obtained using a One-way ANOVA followed by Dunnett's multiple comparisons *post-hoc* test. For the experiments with combination of drugs, statistical significance was obtained using a One-way ANOVA followed by Bonferroni multiple comparisons *post-hoc* test. For the pulse-chase experiments, statistical significance was obtained using a Two-tailed Unpaired *t*-test. Outliers were identified and removed from the analysis by Mean ± (2 × standard deviation).

2.9.3. For the neurosphere growth assay

Neurosphere diameter (D_N, in μm) was measured using the Region of Interest (ROI) Manager tool from (Fiji Is Just) Image J version 2.3.0/1.53q for Windows OS (64-bit). The D_N and the projected area (A_N, in μm^2) of each neurosphere were used as an indirect measure of cell proliferation. The size of the neurospheres was defined as an equivalent circle diameter, $D_N = 2(A_N/\pi)^{1/2}$. Neurospheres of $D_N < 30$ μm were excluded from the analysis because they were mainly single or paired cells. Data is presented as a violin plot with the median, 25% and 75% quartiles or as a bar chart representing the percentage of neurospheres binned according to size. The number of neurospheres considered for analysis in each condition (*n*) is from two independent cell cultures. Normal distribution of data was tested using the Kolmogorov–Smirnov test ($n > 50$) (Mishra et al., 2019). Statistical significance was obtained using a Two-tailed Unpaired *t*-test. For the analysis of the comparison of proportions, statistical significance was obtained using the chi-square test using the MedCalc Software Ltd (2023), according to Campbell (2007) and Richardson (2011). Outliers were identified and removed

from the analysis by Mean ± (2 × standard deviation).

2.9.4. For calcium imaging experiments

Images were collected and analysed using MetaFluor Fluorescence Ratio Imaging Software (Molecular Devices). Regions of interest were acquired by delineating the profile of the cells and averaging the fluorescence intensity inside the delineated area. Statistical significance was obtained after peak determination by the analysis of the area under the curve. Peak amplitudes were calculated by subtracting the baseline level to the maximum peak intensity. Experiments were performed at least in triplicate, except stated otherwise. The number of responsive cells is designated by *n*. A cell was considered responsive when its maximum recorded response was greater than the average of the responses for all cells for each condition. Data is expressed as Mean ± SEM or as a bar chart representing the proportion of responsive vs non-responsive cells. Statistical significance was obtained using a One-way ANOVA followed by Bonferroni multiple comparisons *post-hoc* test. For the analysis of the comparison of proportions, statistical significance was obtained using the chi-square test using the MedCalc Software Ltd (2023), according to Campbell (2007) and Richardson (2011).

3. Results

3.1. TRPV1 expression is increased by CBDV

To evaluate the expression of TRPV1 in our culture model, SVZ neurospheres were incubated for 7 days *in vitro* (DIV7) under differentiative conditions, in the presence or absence of CBDV, and further processed for qRT-PCR. We observed that not only TRPV1 is expressed in SVZ-derived cells, but also its expression is increased in the presence of CBDV, when compared to the control condition ($t_{(6)} = 5.487$, $p = 0.0015$; Ctrl: 1.0-fold; CBDV 1 μM: 2.457 ± 0.363-fold; n = 3–5; ***$p < 0.001$) (Fig. S1).

3.2. CBDV promotes cell viability via a TRPV1-dependent mechanism of action

The effect of CBDV in cell viability was studied using a drug concentration-response curve in SVZ-derived cells. For that, SVZ neurospheres were incubated for 2 days *in vitro* (DIV2) under differentiative conditions with increasing concentrations of CBDV (100 nM - 1 μM) and, 30 min before fixing, cells were incubated with Propidium Iodide (PI) to label late apoptosis or necrosis (Lecoeur, 2002) (Fig. 1A and D).

At DIV2, CBDV-treated cells, at the highest concentration, showed a reduction in the percentage of PI^+ cells when compared to the control condition, therefore promoting cell survival ($F_{(3,12)} = 9$, $p = 0.0016$; Ctrl: 100 ± 0.011%; CBDV 1 μM: 76.63 ± 2.379%; n = 4; **$p < 0.01$) (Fig. 1B and D). To evaluate whether the effects of CBDV upon cell viability were TRPV1-dependent, cells were incubated with the TRPV1 antagonist 5′-iodoresinferotoxin (5′-IRTX) at 300 nM for 30 min, before being co-incubated with the highest concentration of CBDV (1 μM). For CBDV-induced cell survival, the decrease in cell death was blocked in the presence of the antagonist, revealing that CBDV-induced cell survival is TRPV1-dependent ($F_{(3,24)} = 13.24$, $p < 0.0001$; CBDV 1 μM: 73.76 ± 6.068%; 5′-IRTX 300 nM + CBDV 1 μM: 119.4 ± 7.555%; n = 7; §§§§$p < 0.0001$) (Fig. 1C and D). 5′-IRTX alone, in turn, had no effect on cell viability when compared to the control condition (Fig. 1C and D).

Taken together, this data demonstrates that CBDV is able to regulate the viability of SVZ-derived cells via a TRPV1-dependent mechanism of action.

3.3. CBDV promotes cell proliferation in a TRPV1-dependent mechanism of action

To study the effect of CBDV in cell proliferation, SVZ neurospheres were incubated with increasing concentrations of CBDV (100 nM - 1 μM) for DIV2 under differentiative conditions and, 4h before fixing, cells were incubated with 5-bromo-2′-deoxyuridine (BrdU) to label proliferating cells (Fig. 2A and E).

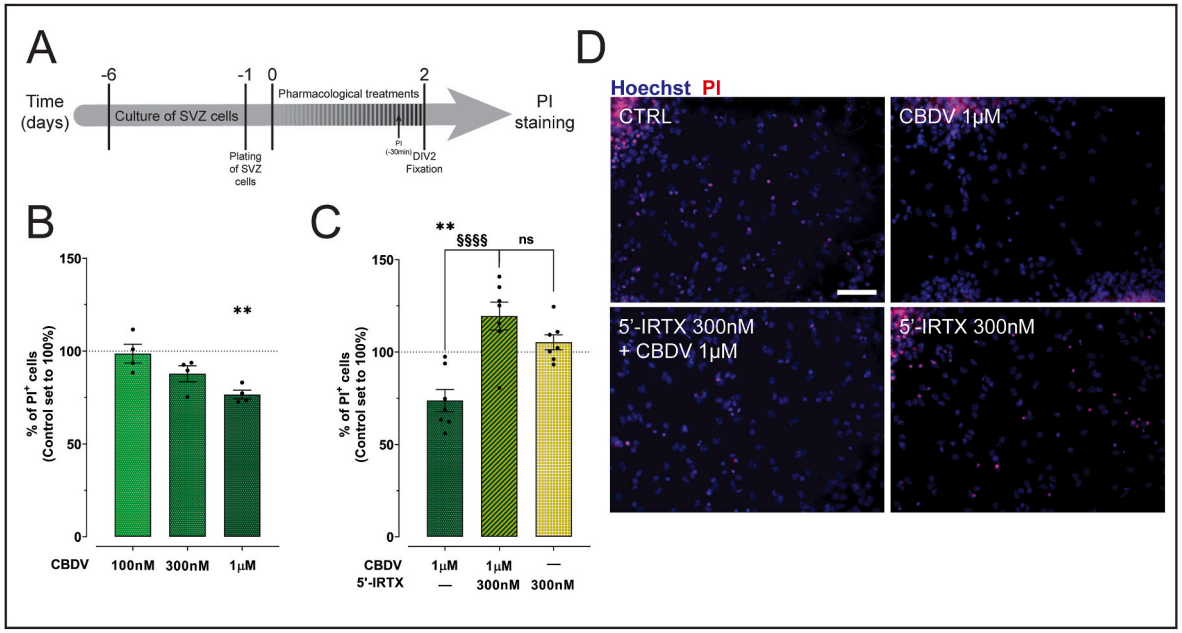

Fig. 1. Cannabidivarin promotes cell viability under differentiative conditions. (A) Schematic representation of the protocol used to evaluate cell viability. **(B)** Bar graphs depict the percentage of PI^+ cells treated with CBDV for DIV2. Values were normalized to the control mean for each experiment. Data presented as Mean ± SEM and the control was set to 100% (corresponding to 15.72% PI^+ cells). n = 4; **p < 0.01. One-way ANOVA using Dunnett's multiple comparison post-hoc test. **(C)** Bar graphs depict the percentage of PI^+ cells co-treated with 5′-iRTX and CBDV for DIV2. Values were normalized to the control mean for each experiment. Data presented as Mean ± SEM and the control was set to 100%. n = 7; ns: p > 0.05; **p < 0.01; §§§§p < 0.0001. One-way ANOVA followed by Bonferroni multiple comparisons post-hoc test. **(D)** Representative fluorescent images of cells positive for PI (in red) and Hoechst 33342 staining (blue nuclei) at DIV2. Scale bar = 50 μm.

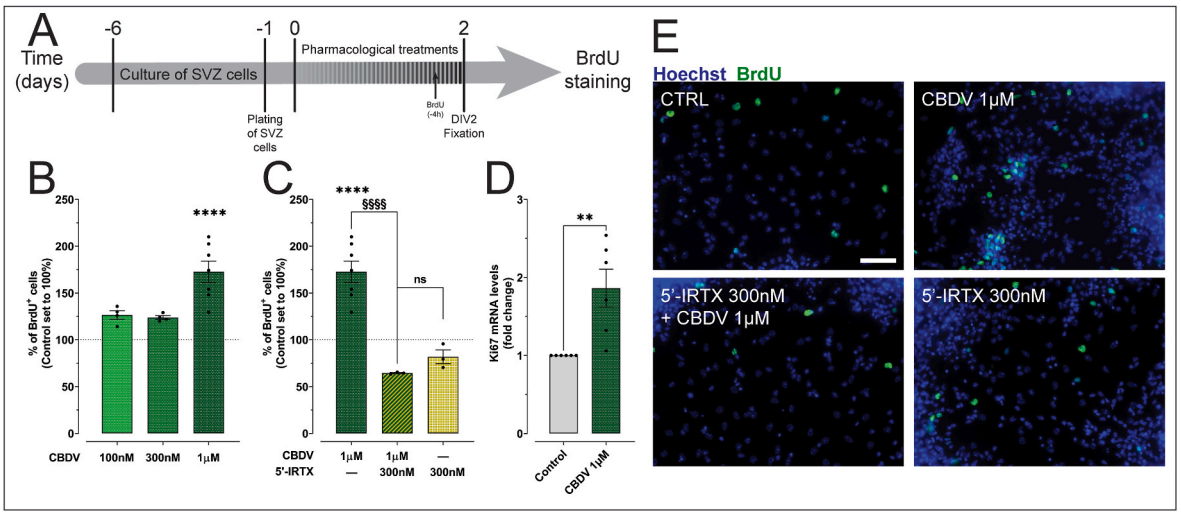

Fig. 2. Cell proliferation is increased with Cannabidivarin-treatment under differentiative conditions. (A) Schematic representation of the protocol used to evaluate cell proliferation. **(B)** Bar graphs depict the percentage of $BrdU^+$ cells treated with CBDV for DIV2. Values were normalized to the control mean for each experiment. Data presented as Mean ± SEM and the control was set to 100% (corresponding to 6.39% $BrdU^+$ cells). n = 4–7; ****p < 0.0001. One-way ANOVA using Dunnett's multiple comparison *post-hoc* test. **(C)** Bar graphs depict the percentage of $BrdU^+$ cells co-treated with 5′-iRTX and CBDV for DIV2. Values were normalized to the control mean for each experiment. Data presented as Mean ± SEM and the control was set to 100%. n = 3–7; ns: p > 0.05; ****p < 0.0001; §§§§p < 0.0001. One-way ANOVA followed by Bonferroni multiple comparisons *post-hoc* test. **(D)** Bar graph depicts the levels of Ki67 mRNA expression. Values were normalized to the control expression of GAPDH expression for each experiment. Data presented as Mean ± SEM and the control was set to 1. n = 6; **p < 0.01. Unpaired *t*-test. **(E)** Representative fluorescent images of cells positive for BrdU (in green) and Hoechst 33342 staining (blue nuclei) at DIV2. Scale bar = 50 μm.

CBDV-treated cells, at the highest concentration, showed an increase in the percentage of $BrdU^+$ cells when compared to the control condition ($F_{(3,18)} = 20.07$, $p < 0.0001$; Ctrl: 100 ± 0.002%; CBDV 1 μM: 172.6 ± 11.360%; n = 4–7; ****$p < 0.0001$) (Fig. 2B and E). Importantly, when the antagonist 5′-IRTX was co-incubated with CBDV, the increase in CBDV-induced cell proliferation was blocked ($F_{(3,16)} = 33.11$, $p < 0.0001$; CBDV 1 μM: 172.6.11 ± 11.360%; 5′-IRTX 300 nM + CBDV 1 μM: 64.36 ± 0.644%; n = 3–7; §§§§$p < 0.0001$) (Fig. 2C and E). Incubation with the antagonist 5′-IRTX alone had no effect on NSPC proliferation (Fig. 2C and E).

To test whether the CBDV-induced proliferative properties in NSPCs were long-lasting and to further assess cell proliferation by a different technique at a different time-point, the expression of Ki67 mRNA, a nuclear protein associated with cellular proliferation, was evaluated in

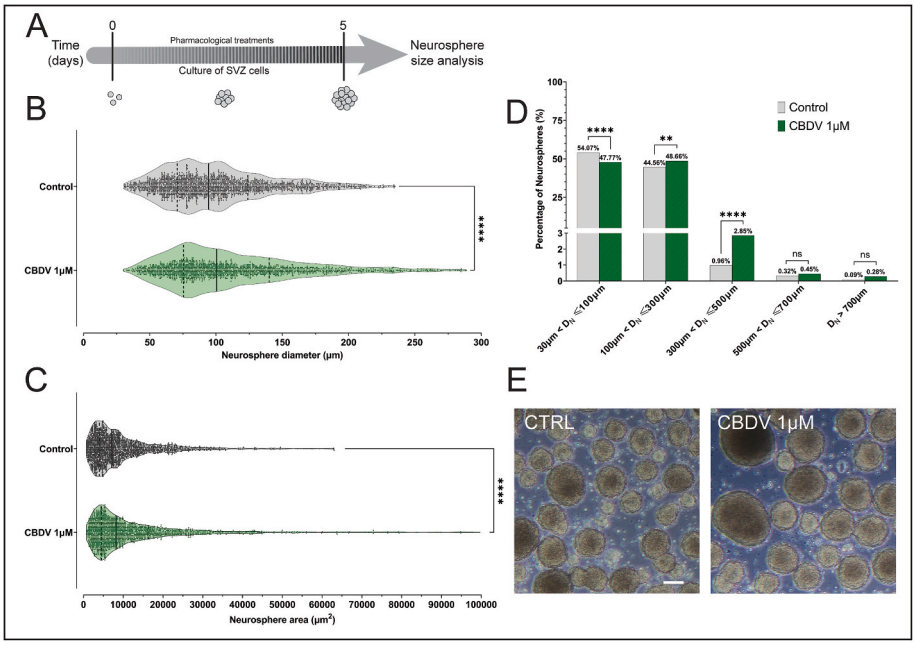

Fig. 3. Neurosphere size is increased with Cannabidivarin-treatment under proliferative conditions. (A) Schematic representation of the protocol used to evaluate neurosphere size. **(B)** Violin plot representing the variation of neurosphere diameter (D_N). Data presented as median, 25% and 75% quartiles. The total number of neurospheres analysed (n) is for Ctrl: 2110, CBDV: 1721, from two independent cultures, ****p < 0.0001. Unpaired *t*-test. **(C)** Violin plot representing the variation of neurosphere area (A_N). Data presented as median, 25% and 75% quartiles. The total number of neurospheres analysed (n) is for Ctrl: 2143, CBDV: 1759, for two independent cultures, ****p < 0.0001. Unpaired *t*-test. **(D)** Bar graph representing the percentages of neurospheres distributed according to the size-binning categories, ns: p > 0.05; **p < 0.01; ****p < 0.0001. Chi-square test. **(E)** Representative phase contrast images of neurospheres after 5 days in culture. Scale bar = 100 μm.

SVZ-derived cells at DIV7. Corroborating the BrdU assays at DIV2, a significant increase in Ki67 expression levels was observed in CBDV-treated cells ($t_{(10)} = 3.552$, $p = 0.0053$; Ctrl: 1.0-fold; CBDV 1 μM: 1.862 ± 0.242-fold; n = 6; $^{**}p < 0.01$) (Fig. 2D).

Furthermore, cell proliferation was also evaluated under proliferative conditions through the assessment of neurosphere size (Fig. 3A and E). In agreement with the results obtained under differentiative conditions, CBDV significantly increased the size of neurospheres, both in terms of diameter (D_N, Fig. 3B) and area (A_N, Fig. 3C), when compared to the control condition (D_N: $t_{(3829)} = 7.658$, $p < 0.0001$; Ctrl: 94.36 (70.81–124.00)μm, n = 2110; CBDV 1 μM: 100.5 (75.49–140.10)μm, n = 1721; $^{****}p < 0.0001$; A_N: $t_{(3900)} = 8.629$, $p < 0.0001$; Ctrl: 7143 (3987–12,526)μm^2, n = 2143; CBDV 1 μM: 8177 (4535–16,195)μm^2, n = 1759; $^{****}p < 0.0001$). A more in-depth analysis of the D_N revealed that CBDV-treated neurospheres generate more neurospheres with a D_N > 300 μm than control condition (X^2 (1, $N = 3969$) = 20.761, $p <$ 0.0001; Ctrl: 1.37%, n = 2177; CBDV 1 μM: 3.58%, n = 1792) (Fig. 3D and E; Table S1).

Thus, these results demonstrate that CBDV promotes cell proliferation in both proliferative and differentiative conditions in a TRPV1-dependent mechanism of action.

3.4. CBDV promotes neuronal differentiation in a TRPV1-dependent mechanism of action

Neuronal differentiation was evaluated in SVZ neurospheres treated with increasing concentrations of CDBV (100 nM - 1 μM), for DIV2 or DIV7, under differentiative conditions. For that, immunocytochemistry (ICC) assays against NeuN, a marker for mature neurons, were performed (Fig. 4A and F).

Our results showed that the highest concentration of CBDV increased the percentage of NeuN$^+$ cells at DIV2, when compared to the control condition ($F_{(3,12)} = 5.422$, $p = 0.0137$; Ctrl: 100 ± 0.006%; CBDV 1 μM: 223.7 ± 44.690%; n = 4; $^{*}p < 0.05$) (Fig. 4B).

Importantly, at DIV7, the effect of the highest concentration of CBDV in neuronal differentiation was still detected ($F_{(3,12)} = 24.67$, $p <$ 0.0001; Ctrl: 100 ± 0.001%; CBDV 1 μM: 264.8 ± 28.930%; n = 4; $^{****}p < 0.0001$) (Fig. 4C and F). Furthermore, at this time point, blocking TRPV1 with 5′-IRTX alone had no significant differences in the percentage of neurons when compared to the control condition. Notwithstanding, CBDV-induced neuronal differentiation was blocked with TRPV1 antagonist ($F_{(3,12)} = 13.83$, $p = 0.0003$; CBDV 1 μM: 228.1 ± 30.480%; 5′-IRTX 300 nM + CBDV 1 μM: 122.1 ± 4.984%; n = 4; §§$p < 0.01$) (Fig. 4D and F).

To further understand the effects of CBDV on the degree of neuronal maturation, the mRNA expression levels of βIII-tubulin, a marker for immature neurons, was evaluated in SVZ neurospheres at DIV7 under differentiative conditions. In fact, in CBDV-treated cells, the mRNA expression of βIII-tubulin was found significantly increased ($t_{(6)} = 8.177$, $p = 0.0002$; Ctrl: 1.0-fold; CBDV 1 μM: 2.263 ± 0.154-fold; n = 4; $^{***}p < 0.001$) (Fig. 4E).

These results highlight the importance of TRPV1 in neuronal

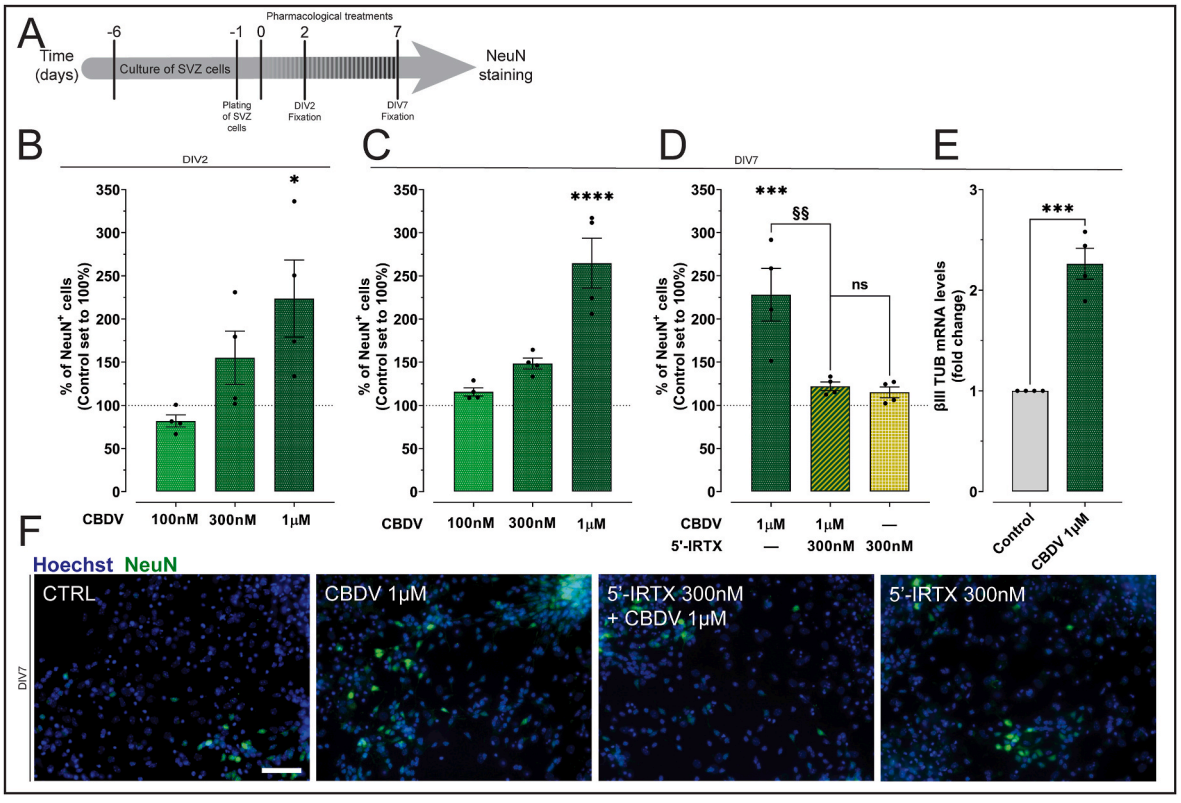

Fig. 4. Neuronal differentiation is increased by Cannabidivarin treatment. (A) Schematic representation of the protocol used to evaluate neuronal differentiation. **(B)** Bar graphs depict the percentage of NeuN$^+$ cells treated with CBDV for DIV2. Values were normalized to the control mean for each experiment. Data presented as Mean ± SEM and the control was set to 100% (corresponding to 3.468% NeuN$^+$ cells). n = 4; *p < 0.05. One-way ANOVA using Dunnett's multiple comparison post-hoc test. **(C)** Bar graphs depict the percentage of NeuN$^+$ cells treated with CBDV for DIV7. Values were normalized to the control mean for each experiment. Data presented as Mean ± SEM and the control was set to 100% (corresponding to 11.143% NeuN$^+$ cells). n = 4; *p < 0.05; ****p < 0.000. One-way ANOVA using Dunnett's multiple comparison post-hoc test. **(D)** Bar graphs depict the percentage of NeuN$^+$ cells co-treated with 5′-IRTX and CBDV for DIV7. Data presented as Mean ± SEM and the control was set to 100%. n = 4; ns: p > 0.05; ***p < 0.0001; §§p < 0.001. One-way ANOVA followed by Bonferroni multiple comparisons post-hoc test. **(E)** Bar graph depicts the levels of βIII-tubulin mRNA expression. Values were normalized to the control expression of GAPDH expression for each experiment. Data presented as Mean ± SEM and the control was set to 1. n = 4; ***p < 0.001. Unpaired *t*-test. **(F)** Representative fluorescent images of cells positive for NeuN (in green) and Hoechst 33342 staining (blue nuclei) at DIV7. Scale bar = 50 μm.

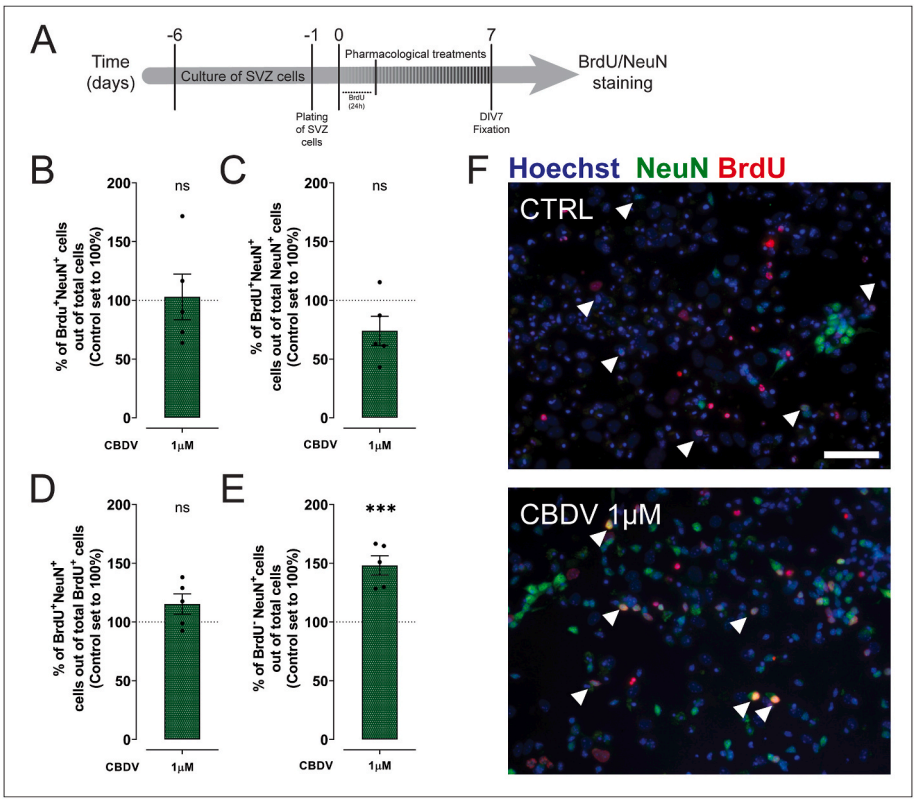

Fig. 5. CBDV promotes NSPC exit of the cell cycle and differentiation into neurons. (A) Schematic representation of the protocol used to evaluate differentiation of neurons from proliferative NSPCs. **(B)** Bar graphs depict the percentage of $BrdU^+NeuN^+$ cells out of total cells. **(C)** Bar graphs depict the percentage of $BrdU^+NeuN^+$ cells out of $NeuN^+$. **(D)** Bar graphs depict the percentage of $BrdU^+NeuN^+$ cells out of $BrdU^+$. **(E)** Bar graphs depict the percentage of $BrdU^-NeuN^+$ out of total cells. **(B–E)** Values were normalized to the control mean for each experiment. Data presented as Mean ± SEM and the control was set to 100% (corresponding to **(B)** 2.490% $BrdU^+NeuN^+$ cells out of total cells; **(C)** 15.731% $BrdU^+NeuN^+$ cells out of $NeuN^+$; **(D)** 38.416% $BrdU^+NeuN^+$ cells out of $BrdU^+$; **(E)** 13.746% $BrdU^-NeuN^+$ out of total cells); n = 5; ns: $p > 0.05$; ***$p < 0.001$. Unpaired *t*-test. **(F)** Representative fluorescent images of cells positive for NeuN (in green), BrdU (in red) and Hoechst 33342 staining (blue nuclei) at DIV 7. Arrows represent double-positive cells for BrdU/NeuN. Scale bar = 50 μm.

differentiation process, namely on its impact in regulating the early stages of NSPC pool and maturation of newborn neurons.

3.5. CBDV-induced neuronal differentiation is a result of cell cycle exit of NSPCs

To further clarify whether the CBDV-induced increase in neuronal differentiation relies on their effects in controlling proliferating and/or cell cycle exit of NSPCs, neurospheres, under differentiative conditions, were subjected to CBDV treatment and exposed to a pulse of BrdU for the first 24h. The drugs, however, remained in culture until DIV7, the time at which cells were co-labelled against BrdU and NeuN (Fig. 5A and F).

Surprisingly no significant changes in the percentage of $BrdU^+NeuN^+$ cells (out of total cells) were observed in CBDV condition ($t_{(8)} = 0.1553$, $p = 0.8804$) (Fig. 5B and F). When looking at the percentage of neurons that differentiated from proliferating cells ($BrdU^+NeuN^+$ cells (out of $NeuN^+$)) (Fig. 5C and F), again no differences were observed ($t_{(8)} = 2.080$, $p = 0.0711$), suggesting that the differentiated $BrdU^+NeuN^+$ neurons represent only a small fraction of the total population of neurons. Concomitantly, when looking at the percentage of proliferating cells that differentiated into neurons ($BrdU^+NeuN^+$ cells (out of $BrdU^+$)) (Fig. 5D and F) no differences were observed when comparing to the control condition ($t_{(8)} = 1.760$, $p = 0.1164$), suggesting that CBDV-induced proliferative cells are not responsible for the increased percentage of neurons observed after this treatment. However, an increase in the percentage of $BrdU^-NeuN^+$ cells (out of total cells) by CBDV treatment was observed ($t_{(8)} = 5.865$, $p = 0.0004$; Ctrl: 100 ± 0.011%; CBDV 1 μM: 148.2 ± 8.213%; n = 5; ***$p < 0.001$), revealing that CBDV induced the arrest and exit of cell cycle in NSPCs and stimulates their differentiation into neurons (Fig. 5E and F).

In conclusion, our BrdU/NeuN experiments clearly show that CBDV-increased $NeuN^+$ cells result from NSPCs that exit the cell cycle.

3.6. CBDV inhibits oligodendrocyte differentiation and maturation

Since cannabinoids have been shown to regulate oligodendrocyte differentiation in the SVZ (Arévalo-Martín et al., 2007), we aimed at understanding if CBDV would share this effect and if TRPV1 was involved. To do so, neurospheres, under differentiative conditions, were treated with CBDV for DIV2 and DIV7, and an ICC against Neuron/glia antigen 2 (NG2), a marker for oligodendrocyte progenitor cells (OPC), was performed (Fig. 6A and F). Notably, CBDV did not induced significant changes in the percentage of $NG2^+$ cells at DIV2 when compared to the control condition ($F_{(3,12)} = 0.1647$, $p = 0.9181$) (Fig. 6B). However, at DIV7, the highest concentration of CBDV ($F_{(3,12)} = 12.12$, $p = 0.0006$; Ctrl: 100 ± 0.011%; CBDV 1 μM: 72.61 ± 3.506%; n = 4; **$p < 0.01$) significantly reduced the percentage of OPCs (Fig. 6C and F). Therefore, given the reduction in the percentage of OPCs, we hypothesized that CBDV could be promoting of oligodendrocyte maturation. Thus, an ICC was performed in the same conditions at DIV7, but this time against Myelin Basic Protein (MBP), a marker for mature myelinating oligodendrocytes (Fig. 6A and G). Surprisingly, the highest concentration of CBDV diminished the percentage of MBP^+ cells ($F_{(3,12)} = 10.80$, $p = 0.0010$; Ctrl: 100 ± 0.004%; CBDV 1 μM: 44.65 ± 3.506%; n = 4; **$p < 0.01$) (Fig. 6D and G).

In addition, and strikingly, blocking TRPV1 with the antagonist 5′-IRTX was able to increase the percentage of MBP^+ cells, when compared to the control condition ($F_{(3,12)} = 13.25$, $p = 0.0004$; Ctrl: 100 ±

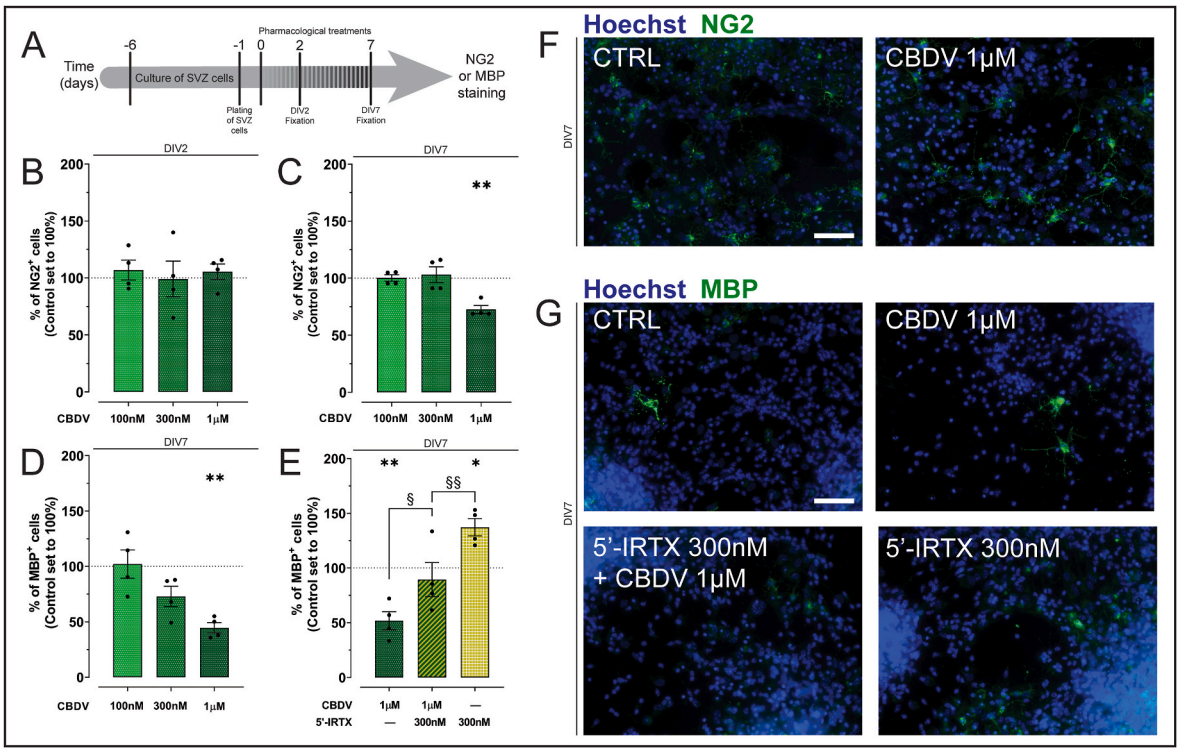

Fig. 6. Oligodendroglial differentiation and maturation is inhibited by Cannabidivarin treatment. (A) Schematic representation of the protocol used to evaluate oligodendrocyte differentiation. **(B)** Bar graphs depict the percentage of $NG2^+$ cells treated with CBDV for DIV2. Values were normalized to the control mean for each experiment. Data presented as Mean ± SEM and the control was set to 100% (corresponding to 13.24% $NG2^+$ cells). n = 4; ns: $p > 0.05$. One-way ANOVA using Dunnett's multiple comparison post-hoc test. **(C)** Bar graphs depict the percentage of $NG2^+$ cells treated with CBDV for DIV7. Data presented as Mean ± SEM and the control was set to 100% (corresponding to 6.943% $NG2^+$ cells). n = 4; **$p < 0.01$. One-way ANOVA using Dunnett's multiple comparison post-hoc test. **(D)** Bar graphs depict the percentage of MBP^+ cells treated with CBDV for DIV7. Data presented as Mean ± SEM and the control was set to 100% (corresponding to 1.395% of MBP^+ cells). n = 4; **$p < 0.01$. One-way ANOVA using Dunnett's multiple comparison post-hoc test. **(E)** Bar graphs depict the percentage of MBP^+ cells co-treated with 5′-IRTX and CBDV for DIV7. Data presented as Mean ± SEM and the control was set to 100%. n = 4; ns: $p > 0.05$; *$p < 0.05$; **$p < 0.01$; §$p < 0.05$; §§$p < 0.01$. One-way ANOVA followed by Bonferroni multiple comparisons post-hoc test. **(F)** Representative fluorescent images of cells positive for NG2 (in green) and Hoechst 33342 staining (blue nuclei) at DIV7. **(G)** Representative fluorescent images of cells positive for MBP (in green) and Hoechst 33342 staining (blue nuclei) at DIV7. Scale bars = 50 μm.

0.001%; 5′-IRTX 300 nM: 137.3 ± 7.918%; n = 4; *$p < 0.05$) (Fig. 6E and G), suggesting that TRPV1 inhibition *per se* promotes MBP differentiation and maturation. As such, when co-incubating 5′-IRTX with CBDV, an increase in the percentage of myelinating oligodendrocytes was detected when comparing with CBDV alone ($F_{(3,12)} = 13.25$, $p = 0.0004$; CBDV 1 μM: 51.81 ± 8.30%; 5′-IRTX 300 nM + CBDV 1 μM: 89.34 ± 15.55%; n = 4; §$p < 0.05$) (Fig. 6E and G).

These results reveal a potential for TRPV1 in the modulation of oligodendrocyte differentiation and maturation.

3.7. CBDV-responsive cells display a two-phase calcium influx profile

Since CBDV acts via TRPV1, a sodium-calcium channel, and that intracellular calcium levels are known regulators of NSPCs fate and neuronal maturation, single cell calcium imaging was performed to evaluate the functional response of SVZ-derived cells at DIV7 exposed, or not (Movie A1) to CBDV. Cells were also exposed to a prior incubation/non-incubation with the TRPV1 antagonist, 5′-ITRX, to further clarify the role of TRPV1 activation in response to these drugs (Fig. 7A).

Surprisingly, incubation with 1 μM CBDV at 100 s elicited two types of calcium influx responses in SVZ-derived cells. One short initial response (≈85 s after the CBDV was added to cells), that corresponds to TRPV1 activation, which is blocked by the antagonist 5′-IRTX, and a second long-lasting response (≈550 s after CBDV was added to cells). Specifically, in the first response, CBDV elicited a moderate increase in the calcium influx, with a peak, followed by a subtle decline ($F_{(3,976)} = 200.5$, $p < 0.0001$; Ctrl peak ratio: 1.014 ± 0.002, n = 365; CBDV 1 μM peak ratio: 1.266 ± 0.026, n = 120 responsive cells; ****$p < 0.0001$). In contrast, in cells co-exposed to CBDV and 5′-IRTX, the initial calcium influx was blocked ($F_{(3,976)} = 200.5$, $p < 0.0001$; CBDV 1 μM peak ratio: 1.266 ± 0.026, n = 120; 5′-IRTX 300 nM + CBDV 1 μM peak ratio: 1.049 ± 0.006, n = 166 responsive cells; §§§§$p < 0.0001$). Unexpectedly, an increase in calcium influx, starting at around 500 s, was also observed, peaking at ≈650s, after CBDV was added, lasting until the end of the experiment. Of note, when compared to the control condition, the co-exposure with the antagonist, resulted in a slight increase of calcium influx at the peak ($F_{(3,976)} = 200.5$, $p < 0.0001$; Ctrl peak ratio: 1.014 ± 0.002, n = 365; 5′-IRTX 300 nM + CBDV 1 μM peak ratio: 1.049 ± 0.006, n = 166 responsive cells; **$p < 0.01$) (Fig. 7B, D, E, F, Movie A2, Movie A4). No significant differences in the calcium profile were detected when comparing the calcium influx of 5′-IRTX exposed cells with the control condition at the peak (Movie A3). Similarly, in the last 100 s of responses, no differences in the calcium influx were observed when comparing control with 5′-IRTX alone (Movie A3). Moreover, the calcium influx induced by CBDV was higher than the influx induced by the co-exposure with the antagonist in the last 100 s of responses ($F_{(3,741)} = 178.9$, $p < 0.0001$; CBDV 1 μM ratio: 1.224 ± 0.016, n = 120; 5′-IRTX 300 nM + CBDV 1 μM: 1.136 ± 0.010, n = 166 responsive cells; §§§§$p < 0.0001$). Furthermore, the influx induced by both CBDV or by co-exposure with the antagonist did not reach levels close to the control baseline in the last 100 s ($F_{(3,741)} = 178.9$, $p < 0.0001$; Ctrl ratio: 0.9964 ± 0.004, n = 365; CBDV 1 μM ratio: 1.224 ± 0.016, n = 120; ****$p <$ 0.0001; 5′-IRTX 300 nM + CBDV 1 μM ratio: 1.136 ± 0.010, n = 166

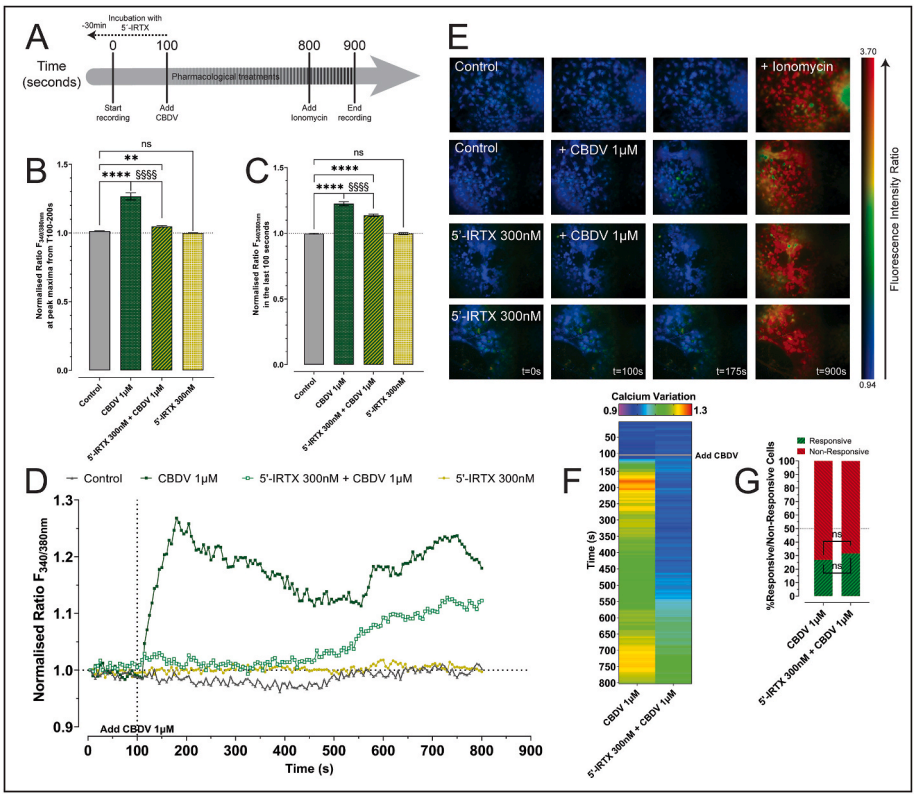

Fig. 7. CBDV-induced calcium influx profile is dependent of TRPV1 activation in SVZ-derived cells. (A) Schematic representation of the protocol used to evaluate calcium influx. **(B)** Ratio of calcium influx at peak maxima from T = 100–200 s, after CBDV exposure. **(C)** Ratio of calcium influx at peak maxima in the last 100s of experiment, after CBDV exposure. **(B) (C)** The responding cells were analysed in each well (120–365 cells) and normalized to the first point of the baseline for each data set. n = 3; ns: $p > 0.05$; **$p < 0.01$; ****$p < 0.01$; §§§§$p < 0.0001$. One-way ANOVA followed by Bonferroni multiple comparisons *post-hoc* test at peak maxima. **(D)** Representative scatter plot that depicts a single-cell variation of calcium influx throughout the time (in seconds) in response to 1 μM CBDV. **(E)** Representative fluorescent intensity ratio of calcium influx (colour code, blue for a low calcium level, green for intermediate, yellow for medium high, and red for high). **(F)** Representative matrix of single-cell calcium response to a pulse of 1 μM CBDV. Each row represents time-points, and the columns represent the mean values of calcium influx of most responsive cells in each condition. The heatmap graph represents a colour-code variation (purple/blue for a low calcium level, green for intermediate, yellow for medium high, and red for high) of the mean values of calcium influx of the most responsive cells from a total of 973 cells analysed in these conditions. **(G)** Stacked bar graphs representing the percentage of responsive versus non-responsive cells influx upon a pulse of 1 μM CBDV. A cell was considered responsive when its maximum recorded response was greater than the average of the responses for all cells for each condition. ns: $p > 0.05$; Chi-square test.

responsive cells; §§§§$p < 0.0001$) (Fig. 7C, D, 7E, 7F, Movie A2, Movie A4).

Interestingly, out of all the analysed cells, no differences were found between the percentage of responsive and non-responsive cells. In more detail, when comparing cells that responded to CBDV to those that were co-incubated with the antagonist, the proportion of responsive cells was equivalent (X^2 (1, $N = 973$) = 0.839, $p = 0.3596$; %Responsive CBDV 1 μM: 26.85%; %Responsive 5′-IRTX 300 nM + CBDV 1 μM: 31.56%). Concomitantly, the proportion on non-responsive cells also presented no differences (X^2 (1, $N = 973$) = 2.580, $p = 0.1082$; %Non-Responsive CBDV 1 μM: 73.15%; %Non-Responsive 5′-IRTX 300 nM + CBDV 1 μM: 68.44%) (Fig. 7G).

In conclusion, CBDV was able to induce two types of response. One, in the first 100s after CBDV exposure, that was blocked by 5′-IRTX, and another that was not blocked by the antagonist in the last 100s of the experimental protocol.

4. Discussion

In this study we describe the proneurogenic effects of CBDV, *in vitro*, as a direct effect of TRPV1 activation. CBDV positively regulates cell survival, cell proliferation and neuronal differentiation in a TRPV1-dependent mechanism of action. Furthermore, inhibition of oligodendrogenesis by CBDV was also observed, which was blocked with TRPV1 antagonist.

Although the affinity of CBDV for TRPV1 is yet uncertain, since the Ki_{TRPV1} for CBDV has not been yet determined, the concentrations of CBDV used in this study were based on previous works made with other endo-, phytho- and synthetic cannabinoids (Compagnucci et al., 2013; Rodrigues et al., 2017; Stanslowsky et al., 2017; Xapelli et al., 2013). In an elegant study by Petrocellis and colleagues (De Petrocellis et al., 2011), they determined the EC_{50} for CBDV for several receptors, namely TRPV1, TRPV2 and TRPA1. Their study has served as the base of several others that further clarified the pharmacology of this drug. Despite that CBDV was reported to have a EC_{50} for TRPA1 (0.42 ± 0.01 μM) lower than for TRPV1 (3.6 ± 0.7 μM), it is possible that these results might be influenced by the methodology applied to determine the EC_{50} (MarÉchal, 2011). In their study, HEK-293 cells were transfected using recombinant rat TRPA1, rat TRPV2 and human TRPV1. While, not only these cells do not physiologically express these receptors (Costanzo et al., 2020; Starkus et al., 2019), the constructs used were from different species, thus the calcium changes, used to determine the EC_{50}, might not totally translate into physiological responses. Furthermore, another study, also using HEK-293 cells, transfected with recombinant human TRPV1, calculated the EC_{50} of CBDV for TRPV1 at 56 μM (Starkus et al., 2019).

While TRPV1 expression in the central nervous system (CNS) has been controversial (reviewed in Kauer and Gibson, 2009), In our model, SVZ-derived cells do not only express high levels of TRPV1, as previously described (Ramírez-Barrantes et al., 2016; Stock et al., 2014; Zhai et al.,

2020), but its mRNA expression is significantly increased in the presence of CBDV. TRPV1 receptors are known to rapidly desensitized once they bind their hypothetical ligands, affecting the pharmacology of this receptor, in particular in prolonged treatments (pharmacological or heat-related) (Touska et al., 2011). In an elegant study by Iannotti and colleagues., they have shown that TRPV1 desensitization elicited by CBDV occurs in concentrations equal or greater than 10 μM (Iannotti et al., 2014). In our study the maximum concentration of CBDV used was 1 μM and, therefore may not elicit the rapid desensitization of TRPV1 as previously described. Furthermore, in our working protocol CBDV was only added once, instead of pulses as described in the article by Iannotti and colleagues. In addition, in our work, the CBDV-induced calcium response was stable only showing a subtle decline, suggesting that desensitization is not playing a major role in the data interpretation.

A not well-understood function of TRPV1 is its role in regulating cell death and proliferation. Particularly, the majority of these studies have been carried out using cancer cell models. These highlighted the potential of several TRPV1 modulators, such as Capsaicin, the prototypic TRPV1 agonist, as inducers of cell death (Díaz-Laviada and Rodríguez-Henche, 2014; Hou et al., 2019; Stock et al., 2012), and inhibitors of cell proliferation (Li et al., 2021; Lin et al., 2013; Weber et al., 2016). Thus, ideal candidates as anti-cancer drugs. In our study, we have found that CBDV, in a TRPV1-dependent manner, was able to promote cell viability and proliferation in SVZ-derived NSPCs. Despite that our data contrasts with what was previously shown using cancer cell lines, it aligns with other works that have evaluated the effects of cannabinoids upon cell death and proliferation (Bockmann et al., 2022; Bravo-Ferrer et al., 2017; Molina-Holgado et al., 2002; Pacher and Mackie, 2012; Rodrigues et al., 2017; Stone et al., 2021; Xapelli et al., 2013; Yang et al., 2020). Interestingly, anandamide, an endogenous cannabinoid and TRPV1 agonist, has been shown to display similar results to the ones obtained in our study (Hofmann et al., 2014; Stock et al., 2012). In fact, regarding cell death, incubation with anandamide alone did not to induce cell death in the GL261 glioma cell line (Stock et al., 2012). In another study, it promoted endothelial cell proliferation in a TRPV1-dependent mechanism of action, since blocking TRPV1 with the antagonist SB366791 inhibited that effect (Hofmann et al., 2014). These works support the idea that TRPV1, via cannabinoids, might play a dual role in the mediation of cell death and cell proliferation.

The transmission of electrical signals between neurons in brain networks and circuits is essential to normal brain function. In an oversimplistic model, the neurosphere assay, cultured NSPCs may differentiate into neurons as a consequence of external neural activity that requires a calcium flux (Deisseroth et al., 2004). Indeed, our work shows that after a 7-day exposure to CBDV, NSPCs exit the cell cycle and differentiate mostly into neurons. While the mechanisms regarding cell cycle arrest induced by TRPV1 have not yet been fully understood, our results further support the idea that CBDV halts NSPC cell cycle. Thus, the modulation of TRPV1 might offer an innovative strategy to study all these important aspects of well-functioning neural precursors.

A recent preprint explored the effects of Cannabidiol (CBD) in a similar experimental paradigm (Romariz et al., 2023). In more detail, Romariz and colleagues showed that CBD, at a concentration of 1 μM had no significant effects on cell viability, with higher concentrations showing to be cytotoxic. Regarding the number and size of neurospheres, at 1 μM there were also no significant differences, suggesting that CBD had no direct effects on NSPC proliferation. Regarding cell differentiation, no differences were also observed regarding the effects of 1 μM CBD on βIII-tubulin immunofluorescent labelled cells, however, a significant decrease was observed for higher concentrations. Despite that CBD and CBDV share some molecular similarities, the pharmacodynamics, the pharmacological targets and consequent downstream signalling cascades, have been shown to be different (reviewed by Alves et al., 2020; Franco et al., 2020). Thus, it is possible that CBDV may also acts via other mechanisms to produce the effects described in this work.

Interestingly, our data has shown that CBDV inhibited oligodendroglial maturation and differentiation. Previous works suggested that oligodendrocyte differentiation and myelinating abilities could be modulated by cannabinoids, which are responsible for promoting OPC survival and maturation (Molina-Holgado et al., 2002; Rodgers et al., 2013). TRPV1 is expressed in OPCs and myelinating oligodendrocytes (Moreno-Luna et al., 2021) suggesting that the development of these cells could be modulated by agonists and antagonists of this channel. Therefore, our results agree with published data whilst not reflecting a positive effect on oligodendrogenesis mediated by cannabinoids. The co-incubation with the antagonist 5′-IRTX, was able to reverse the loss of mature oligodendrocytes induced by CBDV. It should, however, be noted that the percentage of myelinated oligodendrocytes in the presence of both drugs is in between that observed in the presence of each drug alone, therefore additive effects cannot be discarded. Importantly, the incubation of 5′-IRTX alone was able to significantly increase the percentage of myelinating oligodendrocytes. One study linked the effect of 5′-IRTX with the inflammatory response induced my TRPV1 on microglial cells both *in vitro* and in samples of cerebrospinal fluid of patients with multiple sclerosis (MS). Upon incubation with 5′-IRTX, the proinflammatory cytokines tumour necrosis factor and interleukin-6, which were elevated after TRPV1 activation by Capsaicin, were significantly reduced (Bassi et al., 2019). Our data extends these findings by suggesting that 5′-IRTX not only can have anti-inflammatory properties, but also a pro-oligodendrogenic potential. This response of 5′-IRTX can serve up as a proof of concept for future studies aiming at evaluating the neuroimmune modulatory responses of this drug as well as its pro-oligodendrogenic effects in MS. Further studies, clearly outside the scope of this work, are necessary to better understand the role of CBDV as a modulators of oligodendrocyte differentiation and maturation.

One relevant aspect regarding the effects of CBDV upon NSPC modulation was the opposing results regarding neuronal and oligodendroglial differentiation. It is known that the activation of the ERK signalling cascade is necessary to promote neuronal differentiation (Li et al., 2006). TRPV1 ligands can also indirectly influence this pathway via calcium signalling, by phosphorylating and thereby transactivating the epidermal growth factor receptor (EGFR) (Li et al., 2011; Yang et al., 2010). Sustained ERK activation is known to be required for neuronal differentiation (reviewed by Stork, 2003), and, during cortical development, sustained MEK/ERK signalling is necessary for neurogenesis with a concomitant inhibition of gliogenesis (Ménard et al., 2002). In our study, we have shown that upon TRPV1 activation by CBDV we can observe an elevated and prolonged calcium influx, which could be favouring the neuronal path of differentiation with a concurrent inhibition of oligodendrogenesis.

Spontaneous calcium oscillations play important roles in CNS development, neural induction, axon guidance, growth cone morphology, migration, and proliferation (Goswami and Hucho, 2007; Gu et al., 1994; Komuro and Rakic, 1996; Weissman et al., 2004). Regarding CBDV, SVZ-derived cells displayed two types of response, one short initial response that corresponds to TRPV1 activation and which is blocked by prior incubation with 5′-IRTX and a long-lasting response that was not fully blocked by the antagonist, possibly suggesting the involvement of a metabotropic receptor. Therefore, the effects in postnatal SVZ neurogenesis might require the activation of both TRPV1 and a putative metabotropic receptor. This polymodal response corresponds to the initial peak of calcium influx observed, prompted by TRPV1, that might act as a trigger for the adjacent cell responses, which are maintained, long term, via a metabotropic mechanism. Thus, when the antagonist 5′-IRTX is present, the trigger is ablated, and the CBDV-elicited calcium response has a delayed onset, as observed.

Furthermore, one study compared the calcium responses elicited by CBD, to which CBDV is a propyl analogue (Thomas and ElSohly, 2016), with the prototypic TRPV1 agonist Capsaicin (Bisogno et al., 2001). The calcium influx response evoked by Capsaicin was 100-fold higher than the one elicited by CBD (Bisogno et al., 2001). A recent work highlighted

that in cultures derived from rat-dorsal root ganglion neurons, 1 μM of CBD was able to induce a very low calcium response (Anand et al., 2020). In our study, CBDV-elicited a calcium response higher than the CBD reported by Anand and colleagues, and much lower than the one evoked by Capsaicin reported by Bisogno and colleagues. This is relevant since the observed differences regarding the effects of CBDV on cell viability and proliferation might be related to the different magnitudes of calcium influx elicited by different TRPV1 agonists. Indeed, other works have linked the concentration of calcium entering the cell, upon TRPV1 activation, to several molecular pathways that regulate cell homeostasis (Touska et al., 2011; reviewed in Zhai et al., 2020). The pro-apoptotic effects of TRPV1, as seen in cancer studies, may involve the mitochondria (reviewed in Juárez-Contreras et al., 2020). The influx of calcium into the mitochondria results in the depolarization of the mitochondrial membrane and subsequent activation of pro-apoptotic pathways, with higher levels of calcium influx and higher rates of cell death (Kim et al., 2006). On the other hand, TRPV1-dependent cell proliferation has also been linked to ATP release and to the activation of the purine receptor P2Y2, with a limited role for calcium influx (Denda et al., 2010). Neuronal differentiation has been implicated with calcium influx, with increased levels being linked to a faster differentiation and more mature neurons (Holliday et al., 1991; Spoerri et al., 1990). Thus, the concentration of calcium influx elicited by CBDV is critical for the maintenance and regulation of cellular homeostasis, with higher concentrations of calcium leading to cell death and inhibition of cell proliferation, as seen for Capsaicin (reviewed in Zhai et al., 2020), and lower concentrations promoting cell survival, proliferation and a slower rate of differentiation, as suggested for CBDV (Ramírez-Barrantes et al., 2016).

5. Conclusions

Based on the multifactorial responses evoked by CBDV, the data herein described provides new insights on the action of this cannabinoid upon TRPV1, with impact in the modulation of postnatal neurogenesis. Despite that the pharmacodynamics of this cannabinoid are still not entirely clear, there is a strong interest by both researchers and clinicians in repurposing CBDV as a viable medicine, with several clinical trials already undergoing studies for several disorders, ranging from autism spectrum disorders (ClinicalTrials.gov Identifier: NCT03202303, 2017; ClinicalTrials.gov Identifier: NCT03537950, 2018; ClinicalTrials.gov Identifier: NCT03849456, 2019) to androgenetic alopecia (ClinicalTrials.gov Identifier: NCT04842383, 2021). The fact that CBDV is a non-psychoactive cannabinoid with anticonvulsant properties makes this cannabinoid a promising candidate for further studies, particularly in CNS disorders that present alterations in postnatal neurogenesis, such as ASD (Pretzsch et al., 2019; Zamberletti et al., 2021), epilepsy (Huizenga et al., 2019; Zamberletti et al., 2021) and Rett Syndrome (Hurley et al., 2022; Lawson et al., 2018). Given the significant impact of neurological disorders worldwide, the outcome of such studies has the potential to serve as a cornerstone for advancing brain repair strategies by utilizing NSPCs and cannabinoids as therapeutic options.

Ethical statement

All experiments followed the European Community (86/609/EEC; 2010/63/EU; 2012/707/EU) and Portuguese (DL 113/2013) legislation for the protection of animals used for scientific purposes. The protocol was approved by the iMM's institutional Animal Welfare Body – ORBEA-iMM and the National competent authority – DGAV (Direcção Geral de Alimentação e Veterinária) with the number 019075/2016.

Funding information

This work was supported by Fundação para a Ciência e Tecnologia with fellowships PD/BD/141784/2018 and COVID/BD/152658/2022 (DML); PD/BD/128280/2017 (RS); PD/BD/150343/2019 (JM); SFRH/BD/129710/2017 (RR); 2020.04492.BD (JBM). This project has received funding from H2020-WIDESPREAD-05-2020-Twinning (Epi-Epinet) under grant agreement No 952455; International Society for Neurochemistry (ISN) Career Development Grant and International Brain Research Organization (IBRO) Early Career Award.

CRediT authorship contribution statement

Diogo M. Lourenço: Conceptualization, Methodology, Investigation, Formal analysis, Writing – original draft, Writing – review & editing, Visualization. **Rita Soares:** Investigation, Writing – review & editing. **Sónia Sá-Santos:** Methodology, Formal analysis, Writing – review & editing. **Joana M. Mateus:** Investigation, Writing – review & editing. **Rui S. Rodrigues:** Investigation, Writing – review & editing. **João B. Moreira:** Investigation, Writing – review & editing. **Sandra H. Vaz:** Methodology, Writing – review & editing. **Ana M. Sebastião:** Conceptualization, Writing – review & editing, Funding acquisition. **Susana Solá:** Project administration, Writing – review & editing, Funding acquisition. **Sara Xapelli:** Conceptualization, Methodology, Project administration, Writing – original draft, Writing – review & editing, Funding acquisition, Supervision.

Declaration of competing interest

None.

Data availability

Data will be made available on request.

Acknowledgements

The authors would like to thank the Bioimaging Unit of Instituto de Medicina Molecular João Lobo Antunes for their technical support. We also acknowledge the funding PPBI-POCI-01-0145-FEDER-022122. We would also like to thank André Gabriel from the ASB Unit of Instituto de Medicina Molecular João Lobo Antunes, for the valuable insight and knowledge on primer design.

Appendix A. Supplementary data

Supplementary data to this article can be found online at https://doi.org/10.1016/j.ejphar.2023.176079.

Abbreviations

5′-IRTX	5′-iodoresinferotoxin
BrdU	5-bromo-2′-deoxyuridine
CBDV	Cannabidivarin
CB1R	cannabinoid receptor 1
CB2R	cannabinoid receptor 2
DIV	day *in vitro*
ICC	immunocytochemistry
MBP	myelin basic protein
NG2	neuron/glia antigen 2
NSA	neurosphere assay
NSPC	neural stem/progenitor cell
OPC	oligodendrocyte progenitor cell
PI	propidium iodine
qRT-PCR	quantitative real-time reverse transcription polymerase chain reaction
SVZ	subventricular zone
TRPV1	transient receptor potential cation channel subfamily V member 1
NeuN	neuronal nuclei

References

Aguirre, A., Gallo, V., 2004. Postnatal neurogenesis and gliogenesis in the olfactory bulb from NG2-expressing progenitors of the subventricular zone. J. Neurosci. 24, 10530–10541.

Alves, P., Amaral, C., Teixeira, N., Correia-da-Silva, G., 2020. Cannabis sativa: much more beyond Δ9-tetrahydrocannabinol. Pharmacol. Res. 157, 104822.

Anand, U., Jones, B., Korchev, Y., Bloom, S.R., Pacchetti, B., Anand, P., Sodergren, M.H., 2020. CBD effects on TRPV1 signaling pathways in cultured DRG neurons. J. Pain Res. 13, 2269–2278.

Anavi-Goffer, S., Baillie, G., Irving, A.J., Gertsch, J., Greig, I.R., Pertwee, R.G., Ross, R.A., 2012. Modulation of l-α-Lysophosphatidylinositol/GPR55 mitogen-activated protein kinase (MAPK) signaling by cannabinoids. J. Biol. Chem. 287, 91–104.

Arévalo-Martín, Á., García-Ovejero, D., Rubio-Araiz, A., Gómez, O., Molina-Holgado, F., Molina-Holgado, E., 2007. Cannabinoids modulate Olig2 and polysialylated neural cell adhesion molecule expression in the subventricular zone of post-natal rats through cannabinoid receptor 1 and cannabinoid receptor 2. Eur. J. Neurosci. 26, 1548–1559.

Bassi, M.S., Gentile, A., Iezzi, E., Zagaglia, S., Musella, A., Simonelli, I., Gilio, L., Furlan, R., Finardi, A., Marfia, G.A., Guadalupi, L., Bullitta, S., Mandolesi, G., Centonze, D., Buttari, F., 2019. Transient receptor potential vanilloid 1 modulates central inflammation in multiple sclerosis. Front. Neurol. 10, 1–8.

Bisogno, T., Hanus, L., De Petrocellis, L., Tchilibon, S., Ponde, D.E., Brandi, I., Moriello, A.S., Davis, J.B., Mechoulam, R., Di Marzo, V., 2001. Molecular targets for cannabidiol and its synthetic analogues: effect on vanilloid VR1 receptors and on the cellular uptake and enzymatic hydrolysis of anandamide. Br. J. Pharmacol. 134, 845–852.

Bockmann, E.C., Brito, R., Madeira, L.F., da Silva Sampaio, L., de Melo Reis, R.A., França, G.R., Calaza, K. da C., 2022. The role of cannabinoids in CNS development: focus on proliferation and cell death. Cell. Mol. Neurobiol.

Bond, A.M., Ming, G.L., Song, H., 2015. Adult mammalian neural stem cells and neurogenesis: five decades later. Cell Stem Cell 17, 385–395.

Bravo-Ferrer, I., Cuartero, M.I., Zarruk, J.G., Pradillo, J.M., Hurtado, O., Romera, V.G., Díaz-Alonso, J., García-Segura, J.M., Guzmán, M., Lizasoain, I., Galve-Roperh, I., Moro, M.A., 2017. Cannabinoid type-2 receptor drives neurogenesis and improves functional outcome after stroke. Stroke 48, 204–212.

Butti, E., Bacigaluppi, M., Chaabane, L., Ruffini, F., Brambilla, E., Berera, G., Montonati, C., Quattrini, A., Martino, G., 2019. Neural stem cells of the subventricular zone contribute to neuroprotection of the corpus callosum after cuprizone-induced demyelination. J. Neurosci. 39, 5481–5492.

Campbell, I., 2007. Chi-squared and Fisher-Irwin tests of two-by-two tables with small sample recommendations. Stat. Med. 26, 3661–3675.

Caterina, M.J., Schumacher, M.A., Tominaga, M., Rosen, T.A., Levine, J.D., Julius, D., 1997. The capsaicin receptor: a heat-activated ion channel in the pain pathway. Nature 389, 816–824.

Cavallucci, V., Fidaleo, M., Pani, G., 2016. Neural stem cells and nutrients: poised between quiescence and exhaustion. Trends Endocrinol. Metab. 27, 756–769.

Cheung, T.H., Rando, T.A., 2013. Molecular regulation of stem cell quiescence. Nat. Rev. Mol. Cell Biol. 14, 329–340.

ClinicalTrials.gov Identifier: NCT03202303, 2017. Cannabidivarin (CBDV) vs. Placebo in children with autism spectrum disorder (ASD). Montefiore Medical Center.

ClinicalTrials.gov Identifier: NCT03537950, 2018. Shifting Brain Excitation-Inhibition Balance in Autism Spectrum Disorder. King's College London.

ClinicalTrials.gov Identifier: NCT03849456, 2019. Safety and Tolerability of Cannabidivarin (CBDV) in Children and Young Adults with Autism Spectrum Disorder. Pharmaceuticals Jazz.

ClinicalTrials.gov Identifier: NCT04842383, 2021. Androgenetic Alopecia Treatment Using Varin and Cannabidiol Rich Topical Hemp Oil: a Case Series. Gregory L Smith, MD MPH.

Compagnucci, C., Di Siena, S., Bustamante, M.B., Di Giacomo, D., Di Tommaso, M., Maccarrone, M., Grimaldi, P., Sette, C., 2013. Type-1 (CB1) cannabinoid receptor promotes neuronal differentiation and maturation of neural stem cells. PLoS One 8, e54271.

Costanzo, M., Caterino, M., Cevenini, A., Jung, V., Chhuon, C., Lipecka, J., Fedele, R., Guerrera, I.C., Ruoppolo, M., 2020. Dataset of a comparative proteomics experiment in a methylmalonyl-CoA mutase knockout HEK 293 cell model. Data Brief 33, 106453.

Czaja, K., Burns, G.A., Ritter, R.C., 2008. Capsaicin-induced neuronal death and proliferation of the primary sensory neurons located in the nodose ganglia of adult rats. Neuroscience 154, 621–630.

De Petrocellis, L., Ligresti, A., Moriello, A.S., Allarà, M., Bisogno, T., Petrosino, S., Stott, C.G., Di Marzo, V., 2011. Effects of cannabinoids and cannabinoid-enriched Cannabis extracts on TRP channels and endocannabinoid metabolic enzymes. Br. J. Pharmacol. 163, 1479–1494.

Deisseroth, K., Singla, S., Toda, H., Monje, M., Palmer, T.D., Malenka, R.C., 2004. Excitation-neurogenesis coupling in adult neural stem/progenitor cells. Neuron 42, 535–552.

Denda, S., Denda, M., Inoue, K., Hibino, T., 2010. Glycolic acid induces keratinocyte proliferation in a skin equivalent model via TRPV1 activation. J. Dermatol. Sci. 57, 108–113.

Díaz-Laviada, I., Rodríguez-Henche, N., 2014. The potential antitumor effects of capsaicin. In: Abdel-Salam, O.M.E. (Ed.), Capsaicin as a Therapeutic Molecule. Springer Basel, Basel, pp. 181–208.

Ferreira, F.F., Ribeiro, F.F., Rodrigues, R.S., Sebastião, A.M., Xapelli, S., 2018. Brain-derived neurotrophic factor (BDNF) role in cannabinoid-mediated neurogenesis. Front. Cell. Neurosci. 12, 441.

Franco, R., Rivas-Santisteban, R., Reyes-Resina, I., Casanovas, M., Pérez-Olives, C., Ferreiro-Vera, C., Navarro, G., Sánchez de Medina, V., Nadal, X., 2020. Pharmacological potential of varinic-, minor-, and acidic phytocannabinoids. Pharmacol. Res. 158, 104801.

Frey, E., Karney-Grobe, S., Krolak, T., Milbrandt, J., DiAntonio, A., 2018. TRPV1 agonist, capsaicin, induces axon outgrowth after injury via Ca2+/PKA signaling. eNeuro 5, 1–15.

Galve-Roperh, I., Chiurchiù, V., Díaz-Alonso, J., Bari, M., Guzmán, M., Maccarrone, M., 2013. Cannabinoid receptor signaling in progenitor/stem cell proliferation and differentiation. Prog. Lipid Res. 52, 633–650.

Goswami, C., Hucho, T., 2007. TRPV1 expression-dependent initiation and regulation of filopodia. J. Neurochem. 103, 1319–1333.

Goswami, C., Schmidt, H., Hucho, F., 2007. TRPV1 at nerve endings regulates growth cone morphology and movement through cytoskeleton reorganization. FEBS J. 274, 760–772.

Gu, X., Olson, E.C., Spitzer, N.C., 1994. Spontaneous neuronal calcium spikes and waves during early differentiation. J. Neurosci. 14, 6325–6335.

Hill, T.D.M.M., Cascio, M.G., Romano, B., Duncan, M., Pertwee, R.G., Williams, C.M., Whalley, B.J., Hill, A.J., 2013. Cannabidivarin-rich cannabis extracts are anticonvulsant in mouse and rat via a CB1 receptor-independent mechanism. Br. J. Pharmacol. 170, 679–692.

Hofmann, N.A., Barth, S., Waldeck-Weiermair, M., Klec, C., Strunk, D., Malli, R., Graier, W.F., 2014. TRPV1 mediates cellular uptake of anandamide and thus promotes endothelial cell proliferation and network-formation. Biol. Open 3, 1164–1172.

Holliday, J., Adams, R.J., Sejnowski, T.J., Spitzer, N.C., 1991. Calcium-induced release of calcium regulates differentiation of cultured spinal neurons. Neuron 7, 787–796.

Hou, N., He, X., Yang, Y., Fu, J., Zhang, W., Guo, Z., Hu, Y., Liang, L., Xie, W., Xiong, H., Wang, K., Pang, M., 2019. TRPV1 Induced apoptosis of colorectal cancer cells by activating calcineurin-NFAT2-p53 signaling pathway. BioMed Res. Int. 1–9, 2019.

Huizenga, M.N., Sepulveda-Rodriguez, A., Forcelli, P.A., 2019. Preclinical safety and efficacy of cannabidivarin for early life seizures. Neuropharmacology 148, 189–198.

Hurley, E.N., Ellaway, C.J., Johnson, A.M., Truong, L., Gordon, R., Galettis, P., Martin, J. H., Lawson, J.A., 2022. Efficacy and safety of cannabidivarin treatment of epilepsy in girls with Rett syndrome: a phase 1 clinical trial. Epilepsia 63, 1736–1747.

Iannotti, F.A., Hill, C.L., Leo, A., Alhusaini, A., Soubrane, C., Mazzarella, E., Russo, E., Whalley, B.J., Di Marzo, V., Stephens, G.J., 2014. Nonpsychotropic plant cannabinoids, cannabidivarin (CBDV) and cannabidiol (CBD), activate and desensitize transient receptor potential vanilloid 1 (TRPV1) channels in vitro: potential for the treatment of neuronal hyperexcitability. ACS Chem. Neurosci. 5, 1131–1141.

Juárez-Contreras, R., Méndez-Reséndiz, K.A., Rosenbaum, T., González-Ramírez, R., Morales-Lázaro, S.L., 2020. TRPV1 channel: a noxious signal transducer that affects mitochondrial function. Int. J. Mol. Sci. 21, 1–17.

Kauer, J.A., Gibson, H.E., 2009. Hot flash: TRPV channels in the brain. Trends Neurosci. 32, 215–224.

Kee, N., Sivalingam, S., Boonstra, R., Wojtowicz, J., 2002. The utility of Ki-67 and BrdU as proliferative markers of adult neurogenesis. J. Neurosci. Methods 115, 97–105.

Kim, S.R., Kim, S.U., Oh, U., Jin, B.K., 2006. Transient receptor potential vanilloid subtype 1 mediates microglial cell death in vivo and in vitro via Ca 2+ -mediated mitochondrial damage and cytochrome c release. J. Immunol. 177, 4322–4329.

Komuro, H., Rakic, P., 1996. Intracellular Ca2+ fluctuations modulate the rate of neuronal migration. Neuron 17, 275–285.

Kong, K.H., Kim, H.K., Song, K.S., Woo, Y.S., Choi, W.S., Park, H.R., Park, M., Kim, M.E., Kim, M.S., Ryu, J.S., Kim, H.S., Lee, J., 2010. Capsaicin impairs proliferation of neural progenitor cells and hippocampal neurogenesis in young mice. J. Toxicol. Environ. Health Part A Curr. Issues 73, 1490–1501.

Laun, A.S., Shrader, S.H., Brown, K.J., Song, Z.H., 2019. GPR3, GPR6, and GPR12 as novel molecular targets: their biological functions and interaction with cannabidiol. Acta Pharmacol. Sin. 40, 300–308.

Lawson, J.A., Truong, L., Gill, D., Subramanian, G., Cowell, C., 2018. Phase I/II Trial of Cannabidivarin (CBDV) for the Treatment of Epilepsy in Females with Rett Syndrome. American Epilepsy Society.

Lecoeur, H., 2002. Nuclear apoptosis detection by flow cytometry: influence of endogenous endonucleases. Exp. Cell Res. 277, 1–14.

Li, L., Chen, C., Chiang, C., Xiao, T., Chen, Y., Zhao, Y., Zheng, D., 2021. The impact of TRPV1 on cancer pathogenesis and therapy: a systematic review. Int. J. Biol. Sci. 17, 2034–2049.

Li, S., Bode, A.M., Zhu, F., Liu, K., Zhang, J., Kim, M.O., Reddy, K., Zykova, T., Ma, W., Carper, A.L., Langfald, A.K., Dong, Z., 2011. TRPV1-antagonist AMG9810 promotes mouse skin tumorigenesis through EGFR/Akt signaling. Carcinogenesis 32, 779–785.

Li, Z., Theus, M.H., Wei, L., 2006. Role of ERK 1/2 signaling in neuronal differentiation of cultured embryonic stem cells. Dev. Growth Differ. 48, 513–523.

Lin, C.H., Lu, W.C., Wang, C.W., Chan, Y.C., Chen, M.K., 2013. Capsaicin induces cell cycle arrest and apoptosis in human KB cancer cells. BMC Compl. Alternative Med. 13.

Luskin, M.B., Boone, M.S., 1994. Rate and pattern of migration of lineally-related olfactory bulb interneurons generated postnatally in the subventricular zone of the rat. Chem. Senses 19, 695–714.

MarÉchal, E., 2011. Measuring bioactivity: KI, IC50 and EC50. In: Chemogenomics and Chemical Genetics. Springer Berlin Heidelberg, Berlin, Heidelberg, pp. 55–65.

Marques, M.C., Albuquerque, I.S., Vaz, S.H., Bernardes, G.J.L., 2019. Overexpression of osmosensitive Ca2+-permeable channel TMEM63B promotes migration in HEK293T cells. Biochemistry 58, 2861–2866.

MedCalc Software Ltd, 2023. MedCalc's Comparison of Proportions Calculator [WWW Document]. URL. https://www.medcalc.org/calc/comparison_of_proportions.php, 3.29.23.
Ménard, C., Hein, P., Paquin, A., Savelson, A., Yang, X.M., Lederfein, D., Barnabé-Heider, F., Mir, A.A., Sterneck, E., Peterson, A.C., Johnson, P.F., Vinson, C., Miller, F. D., 2002. An essential role for a MEK-C/EBP pathway during growth factor-regulated cortical neurogenesis. Neuron 36, 597–610.
Menn, B., Garcia-Verdugo, J.M., Yaschine, C., Gonzalez-Perez, O., Rowitch, D., Alvarez-Buylla, A., 2006. Origin of oligodendrocytes in the subventricular zone of the adult brain. J. Neurosci. 26, 7907–7918.
Mishra, P., Pandey, C., Singh, U., Gupta, A., Sahu, C., Keshri, A., 2019. Descriptive statistics and normality tests for statistical data. Ann. Card Anaesth. 22, 67.
Molina-Holgado, E., Vela, J.M., Arévalo-Martín, A., Almazán, G., Molina-Holgado, F., Borrell, J., Guaza, C., 2002. Cannabinoids promote oligodendrocyte progenitor survival: involvement of cannabinoid receptors and phosphatidylinositol-3 kinase/akt signaling. J. Neurosci. 22, 9742–9753.
Molina-Holgado, F., Rubio-Araiz, A., García-Ovejero, D., Williams, R.J., Moore, J.D., Arévalo-Martín, Á., Gómez-Torres, O., Molina-Holgado, E., 2007. CB2 cannabinoid receptors promote mouse neural stem cell proliferation. Eur. J. Neurosci. 25, 629–634.
Moreno-Luna, R., Esteban, P.F., Paniagua-Torija, B., Arevalo-Martin, A., Garcia-Ovejero, D., Molina-Holgado, E., 2021. Heterogeneity of the endocannabinoid system between cerebral cortex and spinal cord oligodendrocytes. Mol. Neurobiol. 58, 689–702.
Mori, H., Ninomiya, K., Kino-oka, M., Shofuda, T., Islam, M.O., Yamasaki, M., Okano, H., Taya, M., Kanemura, Y., 2006. Effect of neurosphere size on the growth rate of human neural stem/progenitor cells. J. Neurosci. Res. 84, 1682–1691.
Muller, C., Morales, P., Reggio, P.H., 2019. Cannabinoid ligands targeting TRP channels. Front. Mol. Neurosci.
Pacher, P., Mackie, K., 2012. Interplay of cannabinoid 2 (CB2) receptors with nitric oxide synthases, oxidative and nitrative stress, and cell death during remote neurodegeneration. J. Mol. Med. 90, 347–351.
Pretzsch, C.M., Voinescu, B., Lythgoe, D., Horder, J., Mendez, M.A., Wichers, R., Ajram, L., Ivin, G., Heasman, M., Edden, R.A.E., Williams, S., Murphy, D.G.M., Daly, E., McAlonan, G.M., 2019. Effects of cannabidivarin (CBDV) on brain excitation and inhibition systems in adults with and without Autism Spectrum Disorder (ASD): a single dose trial during magnetic resonance spectroscopy. Transl. Psychiatry 9.
Ramírez-Barrantes, R., Cordova, C., Poblete, H., Muñoz, P., Marchant, I., Wianny, F., Olivero, P., 2016. Perspectives of TRPV1 function on the neurogenesis and neural plasticity. Neural Plast. 2016.
Richardson, J.T.E., 2011. The analysis of 2 × 2 contingency tables-Yet again. Stat. Med. 30, 890–890.
Rodgers, J.M., Robinson, A.P., Miller, S.D., 2013. Strategies for protecting oligodendrocytes and enhancing remyelination in multiple sclerosis. Discov. Med. 16, 53–63.
Rodrigues, R.S., Ribeiro, F.F., Ferreira, F., Vaz, S.H., Sebastião, A.M., Xapelli, S., 2017. Interaction between cannabinoid type 1 and type 2 receptors in the modulation of subventricular zone and dentate gyrus neurogenesis. Front. Pharmacol. 8, 516.
Romariz, S.A.A., Physiology, D., Federal, U., Paulo, D.S., Paulo, S., Physiology, D., Federal, U., Paulo, D.S., Paulo, S., Ribeiro, K., Quintella, M.L., Physiology, D., Federal, U., Paulo, D.S., Paulo, S., 2023. High Doses of Cannabidiol Induce Neurotoxicity in Cell Culture Systems.
Rosenthaler, S., Pöhn, B., Kolmanz, C., Huu, C.N., Krewenka, C., Huber, A., Kranner, B., Rausch, W.-D., Moldzio, R., 2014. Differences in receptor binding affinity of several phytocannabinoids do not explain their effects on neural cell cultures. Neurotoxicol. Teratol. 46, 49–56.
Soares, R., Ribeiro, F.F., Lourenço, D.M., Rodrigues, R.S., Moreira, J.B., Sebastião, A.M., Morais, V.A., Xapelli, S., 2020. Isolation and expansion of neurospheres from postnatal (P1-3) mouse neurogenic niches. J. Vis. Exp.
Spoerri, P.E., Dozier, A.K., Roisen, F.J., 1990. Calcium regulation of neuronal differentiation: the role of calcium in GM1-mediated neuritogenesis. Dev. Brain Res. 56, 177–188.
Stanslowsky, N., Jahn, K., Venneri, A., Naujock, M., Haase, A., Martin, U., Frieling, H., Wegner, F., 2017. Functional effects of cannabinoids during dopaminergic specification of human neural precursors derived from induced pluripotent stem cells. Addiction Biol. 22, 1329–1342.
Starkus, J., Jansen, C., Shimoda, L.M.N., Stokes, A.J., Small-Howard, A.L., Turner, H., 2019. Diverse TRPV1 responses to cannabinoids. Channels 13, 172–191.
Stock, K., Garthe, A., De Almeida Sassi, F., Glass, R., Wolf, S.A., Kettenmann, H., 2014. The capsaicin receptor TRPV1 as a novel modulator of neural precursor cell proliferation. Stem Cell. 32, 3183–3195.
Stock, K., Kumar, J., Synowitz, M., Petrosino, S., Imperatore, R., Smith, E.S.J., Wend, P., Purfürst, B., Nuber, U.A., Gurok, U., Matyash, V., Wälzlein, J.H., Chirasani, S.R., Dittmar, G., Cravatt, B.F., Momma, S., Lewin, G.R., Ligresti, A., De Petrocellis, L., Cristino, L., Di Marzo, V., Kettenmann, H., Glass, R., 2012. Neural precursor cells induce cell death of high-grade astrocytomas through stimulation of TRPV1. Nat. Med. 18, 1232–1238.
Stone, N.L., England, T.J., O'Sullivan, S.E., 2021. Protective effects of cannabidivarin and cannabigerol on cells of the blood-brain barrier under ischemic conditions. Cannabis Cannabinoid Res 6, 315–326.
Stork, P.J.S., 2003. Does Rap1 deserve a bad rap? Trends Biochem. Sci. 28, 267–275.
Straiker, A., Wilson, S., Corey, W., Dvorakova, M., Bosquez, T., Tracey, J., Wilkowski, C., Ho, K., Wager-miller, J., Mackie, K., 2021. An evaluation of understudied phytocannabinoids and their effects in two neuronal models. Molecules 26, 1–17. https://doi.org/10.3390/molecules26175352.
Suzuki, S.O., Goldman, J.E., 2003. Multiple cell populations in the early postnatal subventricular zone take distinct migratory pathways: a dynamic study of glial and neuronal progenitor migration. J. Neurosci. 23, 4240–4250.
Thomas, B.F., ElSohly, M.A., 2016. Biosynthesis and pharmacology of phytocannabinoids and related chemical constituents. In: The Analytical Chemistry of Cannabis. Elsevier, pp. 27–41.
Thornton, C., Dickson, K.E., Carty, D.R., Ashpole, N.M., Willett, K.L., 2020. Cannabis constituents reduce seizure behavior in chemically-induced and scn1a-mutant zebrafish. Epilepsy Behav. 110, 107152.
Tominaga, M., Tominaga, T., 2005. Structure and function of TRPV1. Pflugers Arch. Eur. J. Physiol. 451, 143–150.
Touska, F., Marsakova, L., Teisinger, J., Vlachova, V., 2011. A "cute" desensitization of TRPV1. Curr. Pharmaceut. Biotechnol. 12, 122–129.
Urbán, N., Blomfield, I.M., Guillemot, F., 2019. Quiescence of adult mammalian neural stem cells: a highly regulated rest. Neuron 104, 834–848.
Vilain, S., Esposito, G., Haddad, D., Schaap, O., Dobreva, M.P., Vos, M., van Meensel, S., Morais, V.A., de Strooper, B., Verstreken, P., 2012. The yeast complex I equivalent NADH dehydrogenase rescues pink1 mutants. PLoS Genet. 8.
Wahl, P., Foged, C., Tullin, S., Thomsen, C., 2001. Iodo-resiniferatoxin, a new potent vanilloid receptor antagonist. Mol. Pharmacol. 59, 9–15.
Weber, L.V., Al-Refae, K., Wölk, G., Bonatz, G., Altmüller, J., Becker, C., Gisselmann, G., Hatt, H., 2016. Expression and functionality of TRPV1 in breast cancer cells. Breast Cancer 8, 243–252.
Weissman, T.A., Riquelme, P.A., Ivic, L., Flint, A.C., Kriegstein, A.R., 2004. Calcium waves propagate through radial glial cells and modulate proliferation in the developing neocortex. Neuron 43, 647–661.
Xapelli, S., Agasse, F., Sardà-Arroyo, L., Bernardino, L., Santos, T., Ribeiro, F.F., Valero, J., Bragança, J., Schitine, C., de Melo Reis, R.A., Sebastião, A.M., Malva, J.O., 2013. Activation of type 1 cannabinoid receptor (CB1R) promotes neurogenesis in murine subventricular zone cell cultures. PLoS One 8, e63529.
Yang, H., Wang, Z., Capó-Aponte, J.E., Zhang, F., Pan, Z., Reinach, P.S., 2010. Epidermal growth factor receptor transactivation by the cannabinoid receptor (CB1) and transient receptor potential vanilloid 1 (TRPV1) induces differential responses in corneal epithelial cells. Exp. Eye Res. 91, 462–471.
Yang, S., Hu, B., Wang, Z., Zhang, C., Jiao, H., Mao, Z., Wei, L., Jia, J., Zhao, J., 2020. Cannabinoid CB1 receptor agonist ACEA alleviates brain ischemia/reperfusion injury via CB1–Drp1 pathway. Cell Death Dis. 6.
Zamberletti, E., Rubino, T., Parolaro, D., 2021. Therapeutic potential of cannabidivarin for epilepsy and autism spectrum disorder. Pharmacol. Ther. 226, 107878.
Zhai, K., Liskova, A., Kubatka, P., Büsselberg, D., 2020. Calcium entry through trpv1: a potential target for the regulation of proliferation and apoptosis in cancerous and healthy cells. Int. J. Mol. Sci. 21, 1–25.
Zimmermann, T., Maroso, M., Beer, A., Baddenhausen, S., Ludewig, S., Fan, W., Vennin, C., Loch, S., Berninger, B., Hofmann, C., Korte, M., Soltesz, I., Lutz, B., Leschik, J., 2018. Neural stem cell lineage-specific cannabinoid type-1 receptor regulates neurogenesis and plasticity in the adult mouse hippocampus. Cereb. cortex 28, 4454–4471.